Check for updates

SOFTWARE TOOL ARTICLE

REVISED KSEMAW: an open source software for the analysis of spectrophotometric, ellipsometric and photothermal deflection spectroscopy measurements

[version 2; peer review: 2 approved]

Marco Montecchi[1], Alberto Mittiga[1], Claudia Malerba[1], Francesca Menchini[1,2]

[1]Energy Technologies and Renewable Sources Department, ENEA Research Center Casaccia, Roma, 00123, Italy
[2]Department of Information Engineering, Electronics and telecommunications, University of Roma, Roma, Italy

v2 **First published:** 18 Aug 2021, **1**:95
https://doi.org/10.12688/openreseurope.13842.1
Latest published: 04 Jan 2023, **1**:95
https://doi.org/10.12688/openreseurope.13842.2

Abstract

The optical behavior of devices based on thin films is determined by complex refractive index and thickness of each slab composing the stack; these important parameters are usually evaluated from photometric and/or ellipsometric spectral measurements, given a model of the stack, by means of dedicated software. In the case of complex multilayer devices, generally a number of simpler specimens (like single-film on substrate) must be preliminarily characterized. This paper introduces the reader to a new open source software for thin film characterization finally released after about 30 years of development. The software has already been used in various fields of physics, such as thin film optical filters, architectural glazing, detectors for high energy physics, solar energy, and, last but not least, photovoltaic devices. Code source files, MS Windows executable, user manual as well as a sample of working directories populated with assorted files can be freely downloaded from the kSEMAW GitHub repository.

Keywords

thin film, optical characterization, complex refractive index, film thickness, spectrophotometric measurements, ellipsometric measurements, open source software

H2020 This article is included in the Horizon 2020 gateway.

Open Peer Review

Approval Status ✓ ✓

	1	2
version 2 (revision) 04 Jan 2023		
version 1 18 Aug 2021	✓ view	✓ view

1. **Simone Zanotto**, CNR - Istituto di Nanoscienze, Pisa, Italy

2. **Lars Korte**, Helmholtz-Zentrum Berlin für Materialien und Energie GmbH, Berlin, Germany
Alvaro Tejada, Helmholtz-Zentrum Berlin für Materialien und Energie GmbH, Berlin, Germany
Pontificia Universidad Catolica del Peru, Lima, Peru

Any reports and responses or comments on the article can be found at the end of the article.



This article is included in the Advances in Photonics collection.



This article is included in the Perovskites collection.

Corresponding author: Marco Montecchi (marco.montecchi@enea.it)

Author roles: Montecchi M: Conceptualization, Investigation, Methodology, Software, Supervision, Writing – Original Draft Preparation, Writing – Review & Editing; **Mittiga A**: Conceptualization, Investigation, Methodology, Writing – Original Draft Preparation, Writing – Review & Editing; **Malerba C**: Investigation, Validation, Writing – Original Draft Preparation, Writing – Review & Editing; **Menchini F**: Investigation, Validation, Writing – Original Draft Preparation, Writing – Review & Editing

Competing interests: No competing interests were disclosed.

Grant information: This research was financially supported by the European Union's Horizon 2020 research and innovation programme under the grant agreement Nos 823802 (Solar Facilities for the European Research Area - Third Phase [SFERA-III]) and 952982 (Disruptive Kesterites-Based Thin Film Technologies Customised for Challenging Architectural and Active Urban Furniture Applications [Custom-Art], and the Italian Ministry of Economic Development in the framework of the Operating Agreement with ENEA for the Research on the Electric System.
The funders had no role in study design, data collection and analysis, decision to publish, or preparation of the manuscript.

Copyright: © 2023 Montecchi M *et al*. This is an open access article distributed under the terms of the Creative Commons Attribution License, which permits unrestricted use, distribution, and reproduction in any medium, provided the original work is properly cited.

How to cite this article: Montecchi M, Mittiga A, Malerba C and Menchini F. **KSEMAW: an open source software for the analysis of spectrophotometric, ellipsometric and photothermal deflection spectroscopy measurements [version 2; peer review: 2 approved]** Open Research Europe 2023, **1**:95 https://doi.org/10.12688/openreseurope.13842.2

First published: 18 Aug 2021, **1**:95 https://doi.org/10.12688/openreseurope.13842.1

REVISED **Amendments from Version 1**

Since version 1.0.0:

(a) the whole code is C++ written,

(b) graphs are made with Qwt library,

(c) the simple "Exhaustive Research of solution" replaces the older and harder "Solution Tracking mode",

(d) the standard best-fit of experimental spectra was added,

(e) all kind of experimental spectra can be used in IbridOne and standard best-fit,

(f) a ready-to-use MS Windows executable file is provided.

Any further responses from the reviewers can be found at the end of the article

Plain language summary

kSEMAW software is a useful tool for scientists and technicians dealing with optical devices based on optical coatings. More precisely, kSEMAW is a workspace for the analysis of Spectrophotometric (SP), Ellipsometric (ELI) and Photothermal Deflection Spectroscopy (PDS) measurements. The letter "k" indicates the use of the Qt libraries. Main features: (1) simulate SP, ELI and PDS measurements of a multilayer structure, being known the thicknesses and the complex refractive indexes of each material composing the different layers, (2) calculate the complex refractive index and the thickness of a given layer (if "thin") from experimental measurements (SP, ELI, PDS), being known the thicknesses and the complex refractive indexes of all the other layers composing the structure, (3) evaluate the mean value of physical quantities, weighted on a given international standard spectrum (such as ASTM G173-03) or on own customized reference spectrum, and (4) predict the angular trend by using a realistic model or the equivalent model algorithm.

Introduction

A huge variety of materials can be deposited as films on substrates by means of several well-established techniques, ranging from physical vapour deposition to the simple and economic sol-gel dipping[1]. When the thickness of the film is comparable with the wavelength of an electromagnetic wave hitting the film surface, the transmittance (T) and reflectance (R) of the system are greatly affected by the interference occurring among the contributes originating from the air-film and film-substrate interfaces[2]. This allows, to some extent, regulating transmittance, reflectance and absorptance through an appropriate choice of the type of material composing the film and the film thickness.

As an example the simplest antireflection (AR) coating at the wavelength λ for a transparent window (lens) with refractive index n_{sub} is obtained by depositing a material with refractive index $n \simeq \sqrt{n_{sub}}$, and thickness d satisfying the condition $nd \simeq \lambda/4$; for that reason it is called *quarter wavelength anti-reflection coating*.

In order to shape transmittance and reflectance of the device to an arbitrary structured spectrum, one has to adopt a suitable multi-layer coating, i.e. a stack of several films, where the sequence of different materials and their thicknesses are optimized to get the desired goal.

Thin film technology has become so well established that today everyone, in everyday life, uses many devices based on optical coatings, mono, and multi-layers[1].

Whenever a new material has to be introduced in a coating, its optical characterization is needed to optimize the growth process: as a matter of fact, every deposition set-up is different from another, making the accurate tuning of the many deposition parameters, like vacuum (if needed), temperature, growth rate, etc, mandatory in order to obtain a film sufficiently adherent to the substrate, with the proper refractive index, that is homogeneous all over its surface, is resistant to cleaning, and so on.

Such an optimization process runs by depositing a number of films on one or more substrate types; each specimen has to be optically characterized by measuring its relevant optical features (like T and R at normal or oblique incidence, or the ellipsometric angles Δ and Ψ) from which the complex refractive index of the material and the film thickness are evaluated.

To this aim the software herein presented, under development since 1988, sets an environment where the user can:

- load experimental spectra of different kinds, like photometric, ellipsometric and absorbance detected with a photothermal deflection spectroscopy apparatus (PDS)
- set up an optical model of the sample
- calculate the refractive index and the thickness of the film.

The software is named kSEMAW (Spectro-Ellipsometric Measurement Analysis Workbench), where the letter "k" indicates the use of the Qt libraries to generate the graphical user interface, typical of the Linux KDE desktop environment. Over the years kSEMAW has been expanded to meet the ever-changing needs encountered along the career-path of the corresponding-author, such as:

- optical characterization of thin films[3]
- evaluation of luminous and energetic features of architectural glazing[4]
- optical characterization of scintillator crystal ($PbWO_4$)[5], glue[6] and detector (APD)[7] used in the CMS experiment[8] at LHC of CERN
- optical characterization of mirrors[9] and anti-reflection coatings used in concentrated solar power (CSP)
- last, but not least, optical characterization of tandem photovoltaic cells.

This explains the considerable development that has taken place over the years, accompanied by the replacement of command line with a modern graphic user interface (GUI); this has greatly increased the software ease of use. As a matter of fact, although kSEMAW was born for personal use, like a sort of Swiss knife, the last improvements make it a very interesting tool for anyone working in thin film technology.

Now in this revised version of the paper we describe the new major release of kSEMAW v1.0.0 characterized by the following new main features:

- enterely written in C++ (conversion of all FORTRAN subroutines) with great simplification of its compilation
- new resizable graphs based on Qwt library
- new *Ehaustive Numerical Search Method*, replacing the Solution Tracking one
- new method: Standard Fit of experimental spectra
- improved calculation of the single-layer absorption in multilayers
- availability of the MS Windows executable, ready to use

To add value to the work done so far, believing in knowledge sharing, we took the opportunity offered by Open Research Europe to make kSEMAW available for everyone as open source software under the GNU General Public License as published by the Free Software Foundation version 3. Code source files, user manual as well as a sample of working directories populated with assorted files can be freely downloaded from here.

In this article, after a brief presentation of kSEMAW, rather than replicating the user manual, we will show the main capabilities of the software through concrete examples; all the related files are part of the example working directories, so that interested users can replicate the computing for any example here shown on their own software installation.

What kSEMAW can do

kSEMAW is a workspace for the analysis of Spectrophotometric (SP), Ellipsometric (ELI) and Photothermal Deflection Spectroscopy (PDS) measurements.

kSEMAW allows to:

1. simulate SP, ELI and PDS measurements of a multilayer structure, knowing the thicknesses and the complex refractive indexes $\tilde{n} = n - ik$ of each material composing the different layers[1];

2. calculate the complex refractive index $n - ik$ and the thickness of a given layer (if "thin") from experimental measurements (SP, ELI, PDS), knowing the thicknesses and the complex refractive indexes of all the other layers composing the structure;

3. evaluate the mean value of physical quantities (for example transmittance or reflectance), weighted on a given international standard spectrum (such as the illuminant D65 or the direct solar spectrum ASTM G173-03) or on a customized reference spectrum (for example the crystal scintillator $PbWO_4$ luminescence spectrum, used in the CMS experiment at CERN LHC);

4. predict reflectance/transmittance angular trend, once the realistic model of the coating has been set or by means of the equivalent model algorithm[10]; where necessary output spectra can be weighted over a given reference spectrum.

kSEMAW uses a mathematical approach based on transfer matrices, particularly suitable for the case of multilayers: in addition to being able to treat coherent propagation and interference (for arbitrary incidence angles), it also allows to simulate the effects due to different types of non-ideal material properties, such as optical constants gradients along the film thickness, thickness inhomogeneity, porosity and roughness. The latter is modelled by assuming the thickness to be Gaussian-like distributed with standard deviation σ, and variations along distances much greater than the wavelength λ. The program deals with moderately rough interfaces ($\sigma \ll \lambda$) and limited radiation diffusion[11].

kSEMAW can model devices composed by up to 9 layers of different materials. For each layer it is possible to: i) consider it as optically *thin* or *thick* with respect to the radiation coherence length[2], for summing up coherently or not the contributes originating from its two interfaces in wave propagation; ii) set a refractive index profile along the thickness; iii) introduce roughness at the outermost interface; iv) consider the layer as composed of a mixture of two different materials with optical constants calculated on the basis of the Effective Medium Approximation method. The latter feature can be used to model porosity, by considering the layer as composed by a mixture of material and voids (air) in an given percentage.

Methods

To obtain the unknown n and k values of a film starting from experimental measurements, kSEMAW offers three different methods:

- Exhaustive Numerical search method;
- Standard Fit method;
- Hybrid computational method, called "IbridOne".

Exhaustive Numerical search method

Considered the greatly increased computing power of modern personal computers, the old solution tracking mehod (used in the previous version 0.9.6) no longer has a reason to exist: today *nk*-solutions can be exhaustively computed almost in real time in a pre-selected n-range for each wavelength sampling the experimental spectra.

More precisely the solutions n_λ contained in selected n-range are exhaustively searched by sampling the n range with 101 points; for each one of these n values, the k value that minimizes the merit function $MF = \sum_i (M_{i,cal}(n,k) - M_{i,exp})^2 / \Delta M_i^2$ is found. If the merit function is lower than 1 this (n,k) couple is displayed as a solution. The process is sequentially run over all the wavelengths sampling the wavelength range; a progress-bar informs the user about the status

[1]kSEMAW adopts the convention of negative sign for the imaginary part of both the complex refractive index and dielectric constant; this convention derives from considering the plane wave solution of the Maxwell equations with positive time expressed as $\exp[i(\omega t - \mathbf{q} \cdot \mathbf{r})]$.

[2]According to the Heisenberg uncertainty principle the coherence length is $\Delta l \sim \frac{1}{2\pi}\frac{\lambda^2}{\Delta\lambda}$ where $\Delta\lambda$ is the radiation band-width.

of the process. At the end the found solutions n_λ and k_λ are plotted in two dedicated windows describing a portion of the spaces (λ, n) and (λ, k). Then by observing the set of solutions in the (λ, n) space, one can note that zero, one or more solutions can exist for each wavelength in the case of thin film; in addition, the set of solutions is not necessarily connected. By optimizing the model parameters (thicknesses, roughness, gradients, etc.) according to specific guiding criteria[12,13], a more connected set of solutions can be obtained (see use case #2); finally, among them, a physically reasonable subset of solutions must be selected.

The Exhaustive Numerical Search method typically works on two experimental spectra enabled for the calculation; in the case of a single enabled spectrum, n is set to the value given by an analytical function chosen by the user, while k is found on the basis of the merit function as described before. The recommended combination of spectra are T&R and T&Ψ; the use of only ellipsometric angles could bring to the over-evaluation of k being Δ strongly affected by roughness.

Please note that the solutions found by the Exhaustive Numerical Search only depend on the optical model of the specimen with no need of specific knowledge of the studied material.

Standard Fit method

Differently from the Numerical Search, here the user is asked to model $n(\lambda)$ and $k(\lambda)$ with one or more analytical functions (oscillators) among those offered by the software (see below). Then the selected experimental spectra are best-fitted by optimizing the oscillator and the optical model parameters (thickness, roughness, etc) chosen by the user.

Here a good knowledge of the studied material is fundamental for the reasonable choice of the oscillators for modeling $n(\lambda)$ and $k(\lambda)$.

IbridOne method

In the IbridOne method:

1. $n(\lambda)$ is modelled with appropriate analytical functions;
2. the extinction coefficient $k(\lambda)$ is numerically computed from $T(\lambda)$ and the assumed $n(\lambda)$;
3. the computed reflectance $R_{comp}(\lambda)$ is compared with the experimental one by means of a merit function;
4. some parameters of the assumed $n(\lambda)$ analytical function as well as of the optical model are optimized by a non-linear least square algorithm.

Analytical functions for modelling $n(\lambda)$

Concerning the analytical functions, they may be in principle arbitrary but it is much more convenient that they possess a clear physical interpretation. Theories for the light-matter interaction give expressions for the dielectric susceptibility and the simplest ones are those representing the complex dielectric susceptibility $\tilde{\chi} = \chi_1 - \mathrm{i}\ \chi_2$ associated to single resonant oscillators, obtained from both classical (Drude–Lorentz oscillator) and quantum approach. The dielectric susceptibility is connected to the permittivity $\tilde{\epsilon}$ by the equation

$$\tilde{\epsilon} = \epsilon_1 - \mathrm{i}\epsilon_2 = 1 + \tilde{\chi} = 1 + \chi_1 - \mathrm{i}\chi_2 \tag{1}$$

In turn refractive index and permittivity are both complex quantities connected by the relationships

$$\epsilon_1 = n^2 - k^2, \qquad \epsilon_2 = 2nk \tag{2}$$

and inversely

$$n = \frac{1}{\sqrt{2}}\sqrt{\sqrt{\epsilon_1^2 + \epsilon_2^2} + \epsilon_1}, \qquad k = \frac{1}{\sqrt{2}}\sqrt{\sqrt{\epsilon_1^2 + \epsilon_2^2} - \epsilon_1} \tag{3}$$

In the current version, kSEMAW can model the dependence of the refractive index on wavelength $n(\lambda)$ using up to 20 “oscillators” (i.e. analytical functions) belonging to the following 9 classes:

- Flat
- Lorentz
- Quant-homo

- Quant-inhomo
- Drude
- Direct Gap Cody
- Direct Gap Tauc
- Indirect Gap Cody
- Indirect Gap Tauc

kSEMAW calculates the total $\tilde{\epsilon}$ adding up the susceptibilities of all the selected oscillators. The complex refractive index will be then calculated using Equation 3.

The oscillator functions are described in detail in Appendix A of the user manual available in the kSEMAW GitHub repository[14]. Here we just give a brief description for each one.

The "Flat" oscillator is a simple real constant. One "Flat" oscillator must be always inserted to take into account the term "1" in Equation 1 (i.e. the vacuum permittivity ϵ_0) as well as the tail-contribution of the transitions at high energies, out of the investigated wavelength range, and not explicitly considered.

The "Lorentz" oscillator is based on the classic Lorentz oscillator formula[15]:

$$\tilde{\chi}_{lo} = C\left[\frac{(E_r^2 - E^2)}{(E_r^2 - E^2)^2 + (ED)^2} - \mathrm{i}\frac{ED}{(E_r^2 - E^2)^2 + (ED)^2}\right] \tag{4}$$

where C is the oscillator amplitude, E_r is the resonance energy and D is the line width.

The "Quant-homo" oscillator is based on the simple quantum oscillator formulas[16] valid for the case of homogeneous broadening and its shape is given by:

$$\tilde{\chi}_{qo}(E, E_r) = C\left[\frac{(E_r - E)/D}{1 + [(E_r - E)/D]^2} - \mathrm{i}\frac{1}{1 + [(E_r - E)/D]^2}\right] \tag{5}$$

As reported in 17, the "Quant-homo" oscillator formula is obtained by neglecting a not-resonant term in the quantum treatment (otherwise a formula practically equivalent to the Lorentz oscillator would be obtained). This approximation is excellent near the resonance energy while a small difference appears far away from it. On the other hand the simple and elegant equations obtained with this approximation will be quite useful in the following.

When the absorbing centres in a material cannot be considered as identical replicas, the absorption-line broadening is inhomogeneous. For example absorbing centres may be slightly different in a crystal because of random presence of strain or proximity to other lattice defects and impurities that are randomly distributed. "Quant-inhomo" is therefore obtained by making the convolution between a homogeneous quantum oscillator and a Gaussian distribution centred in E_r and with half width at half maximum (HWHM) equal to D[18]; the line width of the homogeneous quantum oscillator is assumed to be much lower than the Gaussian one.

The "Drude" oscillator describes the response of a free electron gas and can be obtained by setting $E_r = 0$ in the "Lorentz" oscillator:

$$\tilde{\chi}_{dr} = -\frac{E_0^2}{D^2 + E^2} - \mathrm{i}\frac{E_0^2 D}{E(D^2 + E^2)}. \tag{6}$$

In this case, D is related to the carrier scattering time τ by $D = \hbar/\tau$ while E_0 is given by $E_0^2 = (\hbar N q^2)/(m^* \epsilon_0)$ where N is the carrier density per unit volume and m^* is the carrier effective mass.

These single resonant oscillators are unsuitable to describe the optical constants of systems with a continuous distribution of density of states such as semiconductors; therefore the last four functions, specific for semiconductor materials, have been added and treated with a new approach.

As a matter of fact the semiconductors theories reported in textbooks[19] usually derive $\epsilon_2 = \chi_2$ only and exclusively at energies near the fundamental gap. Furthermore the calculation is made by hypothesizing that the excited states have infinite lifetime, i.e. that every transition between two states may take place only by absorbing photons with energy exactly equal to the difference of their energetic levels; the real part ϵ_1 is not explicitly calculated, but it can be obtained by means of the Kramers-Kronig relations. Since the Kramers-Kronig integrals have to be numerically computed (except for particular cases) that approach is not so convenient for best-fit procedures.

In kSEMAW analytical expressions for both χ_1 and χ_2, satisfying the Kramers-Kronig relations and having a clear physical interpretation, are used. These expressions are obtained performing the convolution between a suitable χ_2^{inf} calculated for infinite lifetime and the normalized ($C = 1/(\pi D)$) complex $\tilde{\chi}_{qo}$ describing the response of a quantum oscillator (Equation 5):

$$\tilde{\chi}(E) = \int \chi_2^{inf}(E_r)\tilde{\chi}_{qo}(E_r - E)dE_r \tag{7}$$

The result of the convolution can be expressed as analytical functions in a few simple but interesting cases discussed below.

In general χ_2^{inf} can be expressed as the product of the joint density of states $\rho(E)$ and a transition intensity $I(E)$[20]:

$$\chi_2^{inf}(E) = I(E)\rho(E) \tag{8}$$

$I(E)$ contains the squared modulus of the matrix element of the electron-photon interaction Hamiltonian between the initial and final states. In the dipole approximation the Hamiltonian is proportional to the position operator (r) but it can be written in an equivalent way using the momentum operator (p) also. A relation between the matrix elements of these two operators can be obtained using commutator relations:

$$\left|\langle p\rangle\right|^2 = \left|\langle r\rangle\right|^2\left(\frac{mE}{\hbar}\right)^2 \tag{9}$$

The energy dependence of $I(E)$ cannot be easily predicted and therefore it is assumed to be a constant if $|\langle r\rangle|^2$ is supposed to be independent of energy while it is assumed to be proportional to $1/E^2$ if $|\langle p\rangle|^2$ is supposed to be independent of energy. The constant $|\langle p\rangle|^2$ assumption was used by Tauc *et al.*[21] in the interpretation of the optical absorption of amorphous semiconductors leading to the well known "Tauc plot" method to derive the optical gap. The constant $|\langle r\rangle|^2$ assumption was later on proposed by Cody[22] again for the amorphous semiconductor case. These two alternatives can be used for crystalline materials too. For example in crystalline GaAs the energy dependence of the optical absorption above the bandgap is better described by the constant position matrix element[20] rather than by the more commonly hypothesized constant momentum matrix element.

For a crystalline semiconductor with direct allowed transitions between two parabolic bands separated by an energy gap E_0, $\rho(E)$ can be written as[19]:

$$\rho(E) = C_r(E - E_0)^{1/2} \tag{10}$$

This monotonically increasing expression for $\rho(E)$ is obviously valid only for energies slightly larger than the gap. For higher energy values $\rho(E)$ can show a rather complex behavior but it has also a high energy limit determined by the extension of the valence and conduction bands. At the gap E_0 and at this high energy limit (E_3) the $\rho(E)$ has two "critical points" called $M0$ and $M3$ where it goes to zero following a square root behavior[19].

The simplest expression valid for every energy which has the correct square root behaviour near E_0 and E_3 is:

$$\rho(E) = C_r\sqrt{(E - E_0)(E_3 - E)} \tag{11}$$

Using this expression and the "Cody's approximation" the χ_2^{inf} also has the same form:

$$\chi_{2-dir-Cody}^{inf}(E) = C\sqrt{(E - E_0)(E_3 - E)} \tag{12}$$

Equation 12 can be considered as an acceptable approximation for $\chi_2^{inf}(E)$ in the case of a direct gap material with position matrix element independent of energy and with infinite lifetime (see Figure 1a).

On the other hand in Tauc's approximation, the momentum matrix element is considered independent of energy and therefore, as previously discussed, the transition intensity is proportional to $1/E^2$ (see Figure 1b), thus:

$$\chi_{2-dir-Tauc}^{inf}(E) = C\frac{\sqrt{(E-E_0)(E_3-E)}}{E^2} \tag{13}$$

Other types of critical points do exist ($M1$ and $M2$) in the $\rho(E)$[19], but they are not yet included among the fitting functions of kSEMAW.

Both the complex permittivity components for these two cases can be obtained by the convolution between the functions in Equation 12 and Equation 13 and the normalized quantum oscillator $\tilde{\chi}_{qo}$.

Direct gap Cody:

$$\chi_{1-dir-Cody}(E) = \frac{CD}{2}\left\{a+b-2(a^2+1)^{1/4}(b^2+1)^{1/4}\cos\left[\frac{1}{2}\arctan\left(\frac{1}{a}\right)+\frac{1}{2}\arctan\left(\frac{1}{b}\right)\right]\right\}$$
$$= \frac{CD}{2}\left[a+b-2\Re\left(\sqrt{a+i}\sqrt{b+i}\right)\right] \tag{14}$$

$$\chi_{2-dir-Cody}(E) = -CD\left\{1+(a^2+1)^{1/4}(b^2+1)^{1/4}\sin\left[\frac{1}{2}\arctan\left(\frac{1}{a}\right)+\frac{1}{2}\arctan\left(\frac{1}{b}\right)\right]\right\}$$
$$= -CD\left[1-\Im\left(\sqrt{a+i}\sqrt{b+i}\right)\right] \tag{15}$$

where $a = \frac{E_0-E}{D}$ and $b = \frac{E_3-E}{D}$.

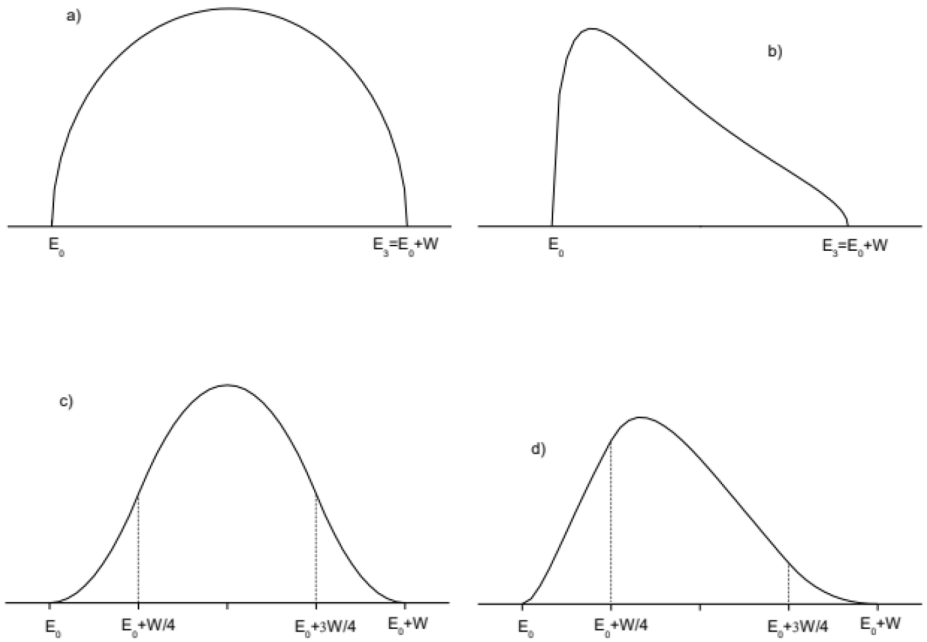


Figure 1. Imaginary part of the dielectric susceptibility for infinite lifetime semiconductor (χ_2^{inf}) and: **a**) direct gap under Cody's approximation **b**) direct gap under Tauc's approximation, **c**) indirect gap under Cody's approximation **d**) indirect gap under Tauc's approximation. E_0 is the semiconductor gap. The high energy limit of the absorption band is labelled as E_3=E_0+W where W is the absorption band width.

Direct gap Tauc

$$\chi_{1-dir-Tauc}(E)=\frac{C}{2D}\Re\left\{\frac{1}{2(D-iE)}\left(2iD+2E-2\sqrt{E_0E_3}-(i-1)\sqrt{2}\sqrt{D-i(E-E_0)}\sqrt{-iD-E+E_3}\right)+\frac{1}{2(D+iE)}\left(-2iD+2E-2\sqrt{E_0E_3}+(i+1)\sqrt{2}\sqrt{D+i(E-E_0)}\sqrt{iD-E+E_3}\right)+E(D-iE)^2\sqrt{D+i(E-E_0)}\sqrt{D+i(E-E_3)}/\left(D^2+E^2\right)^2+E(D+iE)^2\sqrt{D-i(E-E_0)}\sqrt{D-i(E-E_3)}/\left(D^2+E^2\right)^2-ED\left(D^2(E_0+E_3)+E(-4E_0E_3+E(E_0+E_3))\right)/\left(\left(D^2+E^2\right)^2\sqrt{E_0E_3}\right)\right\} \quad (16)$$

$$\chi_{2-dir-Tauc}(E)=CD\Re\left\{-\left[(D-iE)^2\sqrt{D+i(E-E_0)}\sqrt{D+i(E-E_3)}\right]/\left(2D\left(D^2+E^2\right)^2\right)-\left[(D+iE)^2\sqrt{D-i(E-E_3)}\sqrt{D-i(E-E_0)}\right]/\left(2D\left(D^2+E^2\right)^2\right)+D\left[D^2(E_0+E_3)+E(-4E_0E_3+E(E_0+E_3))\right]/\left(2D\left(D^2+E^2\right)^2\sqrt{E_0E_3}\right)\right\} \quad (17)$$

Different formulas must be used for materials where the fundamental gap is due to indirect transitions: in this case the excitation process includes the absorption or the emission of a phonon necessary to allow transitions between electronic states with different crystalline momentum. The absorption/emission of phonons removes the momentum conservation constraint and therefore for indirect transitions $\rho(E)$ is proportional to the convolution of the density of states of the two bands. In amorphous semiconductors also the momentum conservation is not required because the disorder destroys translational simmetry and momentum is no more a good quantum number. It follows that oscillators for indirect transitions in crystalline semiconductors can be used to fit the optical constants of amorphous semiconductors too.

Analytical expressions for the convolution integral over the whole bands are not available, but it is well known that the convolution between two square root densities of states gives a function which increases parabolically above the gap. Therefore an empirical approximated expression can be obtained by joining two parabolic edges with a parabolic maximum, getting in Cody's approximation (see Figure 1c):

$$\chi^{inf}_{2-ind-Cody}(E)=\frac{16C}{\mathrm{W}^2}(E-E_0)^2 \quad \text{if } E_0<E<E_0+\mathrm{W}/4 \quad (18)$$

$$\chi^{inf}_{2-ind-Cody}(E)=C\left\{2-\frac{16}{\mathrm{W}^2}[E-(E_0+\mathrm{W}/2)]^2\right\} \quad \text{if } E_0+\frac{\mathrm{W}}{4}<E<E_0+\frac{3\mathrm{W}}{4} \quad (19)$$

$$\chi^{inf}_{2-ind-Cody}(E)=\frac{16C}{\mathrm{W}^2}[E-(E_0+\mathrm{W})]^2 \quad \text{if } E_0+\frac{3\mathrm{W}}{4}<E<E_0+\mathrm{W} \quad (20)$$

where E_0 is the gap energy and W is the absorption band width.

In the Tauc's approximation the above expressions must be divided by the term E^2.

As for the direct gap case, both the complex permittivity components can be obtained by the convolution between these parabolic terms and the normalized quantum oscillator $\tilde{\chi}_{qo}$.

Indirect gap-Cody

$$\begin{aligned}\chi_{1-ind-Cody}(E) = C\{&2IC_{Re}^{Cody}(E, E_0 + 3\mathrm{W}/4) - 2IC_{Re}^{Cody}(E, E_0 + \mathrm{W}/4) + \\ &16/\mathrm{W}^2[+I2_{Re}^{Cody}(E, E_0, E_0 + \mathrm{W}/4) - I2_{Re}^{Cody}(E, E_0, E_0) \\ &- I2_{Re}^{Cody}(E, E_0 + \mathrm{W}/2, E_0 + 3\mathrm{W}/4) + I2_{Re}^{Cody}(E, E_0 + \mathrm{W}/2, E_0 + \mathrm{W}/4) \\ &+ I2_{Re}^{Cody}(E, E_0 + \mathrm{W}, E_0 + \mathrm{W} - I2_{\mathrm{Re}}^{Cody}(E, E_0 + \mathrm{W}, E_0 + 3\mathrm{W}/4]\}\end{aligned} \tag{21}$$

where:

$$IC_{Re}^{Cody}(E, E_r) = \frac{1}{\pi D}\int \frac{[(E_r - E)/D]\,\mathrm{d}E_r}{1 + [(E_r - E)/D]^2} = \frac{1}{2\pi}\ln\left[D^2 + (E - E_r)^2\right] \tag{22}$$

$$\begin{aligned}I2_{Re}^{Cody}(E, E_0, E_r) = \frac{1}{\pi D}\int \frac{(E_r - E_0)^2[(E_r - E)/D]\,\mathrm{d}E_r}{1 + [(E_r - E)/D]^2} = \\ \frac{1}{2\pi}\left\{(E_r - E)(3E - 4E_0 + E_r) + 4D(E - E_0)\arctan\left(\frac{E - E_r}{D}\right)\right. \\ \left. + [(E - E_0)^2 - D^2]\ln\left[D^2 + (E - E_r)^2\right]\right\}\end{aligned} \tag{23}$$

$$\begin{aligned}\chi_{2-ind-Cody}(E) = C\{&2IC_{Im}^{Cody}(E, E_0 + 3\mathrm{W}/4) - 2IC_{Im}^{Cody}(E, E_0 + \mathrm{W}/4) + \\ &16/\mathrm{W}^2[+I2_{Im}^{Cody}(E, E_0, E_0 + \mathrm{W}/4) - I2_{Im}^{Cody}(E, E_0, E_0) \\ &- I2_{Im}^{Cody}(E, E_0 + \mathrm{W}/2, E_0 + 3\mathrm{W}/4) + I2_{Im}^{Cody}(E, E_0 + \mathrm{W}/2, E_0 + \mathrm{W}/4) \\ &+ I2_{Im}^{Cody}(E, E_0 + \mathrm{W}, \quad E_0 + \mathrm{W}) - \quad I2_{Im}^{Cody}(E, E_0 + \mathrm{W}, E_0 + 3\mathrm{W}/4)]\}\end{aligned} \tag{24}$$

Where:

$$IC_{Im}^{Cody}(E, E_r) = \frac{1}{\pi D}\int \frac{\mathrm{d}E_r}{1 + [(E_r - E)/D]^2} = -\frac{1}{\pi}\arctan\left(\frac{E - E_r}{D}\right) \tag{25}$$

$$\begin{aligned}I2_{Im}^{Cody}(E, E_0, E_r) = \frac{1}{\pi D}\int \frac{(E_r - E_0)^2\,\mathrm{d}E_r}{1 + [(E_r - E)/D]^2} = \frac{1}{\pi}\left(\left[D^2 + (E - E_0)^2\right]\arctan\left(\frac{E - E_r}{D}\right)\right. \\ \left. + D\left\{E_r - E + (E - E_0)\ln\left[D^2 + (E - E_r)^2\right]\right\}\right)\end{aligned} \tag{26}$$

Indirect gap-Tauc

$$\begin{aligned}\chi_{1-ind-Tauc}(E) = C\{&2IC_{Re}^{Tauc}(E, E_0 + 3\mathrm{W}/4) - 2IC_{Re}^{Tauc}(E, E_0 + \mathrm{W}/4) + \\ &16/\mathrm{W}^2[+I2_{Re}^{Tauc}(E, E_0, E_0 + \mathrm{W}/4) - I2_{Re}^{Tauc}(E, E_0, E_0) \\ &- I2_{Re}^{Tauc}(E, E_0 + \mathrm{W}/2, E_0 + 3\mathrm{W}/4) + I2_{Re}^{Tauc}(E, E_0 + \mathrm{W}/2, E_0 + \mathrm{W}/4) \\ &+ I2_{Re}^{Tauc}(E, E_0 + \mathrm{W}, \quad E_0 + \mathrm{W}) \quad - I2_{Re}^{Tauc}(E, E_0 + \mathrm{W}, \quad E_0 + 3\mathrm{W}/4)]\}\end{aligned} \tag{27}$$

where:

$$\begin{aligned}IC_{Re}^{Tauc}(E, E_r) = \frac{1}{\pi D}\int \frac{[(E_r - E)/D]\,\mathrm{d}E_r}{E_r^2[1 + [(E_r - E)/D]^2]} = \\ \frac{1}{2\pi(D^2 + E^2)^2}\left(-4DE\arctan\left(\frac{E - E_r}{D}\right) + \frac{2E(D^2 + E^2)}{E_r} + (E^2 - D^2)\ln\left(\frac{D^2 + (E - E_r)^2}{E_r^2}\right)\right\}\end{aligned} \tag{28}$$

$$I2_{Re}^{Tauc}(E,E_0,E_r)=\frac{1}{\pi D}\int\frac{(E_r-E_0)^2[(E_r-E)/D]\,\mathrm{d}E_r}{E_r^2[1+[(E_r-E)/D]^2]}=\frac{1}{2\pi(D^2+E^2)^2}\left\{4DE_0(D^2+E^2-EE_0)\arctan\left(\frac{E-E_r}{D}\right)\right.$$
$$+[D^4+E^2(E-E_0)^2+D^2(2E^2-2EE_0-E_0^2)]\ln(D^2+(E-E_r)^2)$$
$$\left.+2E_0\left[\frac{E(D^2+E^2)E_0}{E_r}+(E^2(2E-E_0)+D^2(2E-E_0))\ln(E_r)\right]\right\} \quad (29)$$

$$\chi_{2-ind-Tauc}(E)=C\{2IC_{Im}^{Tauc}(E,E_0+3\,\mathrm{W}/4)-2IC_{Im}^{Tauc}(E,E_0+\mathrm{W}/4)+$$
$$16/\mathrm{W}^2[+I2_{Im}^{Tauc}(E,E_0,E_0+\mathrm{W}/4)-I2_{Im}^{Tauc}(E,E_0,E_0)$$
$$-I2_{Im}^{Tauc}(E,E_0+\mathrm{W}/2,E_0+3\,\mathrm{W}/4)+I2_{Im}^{Tauc}(E,E_0+\mathrm{W}/2,E_0+\mathrm{W}/4)$$
$$+I2_{Im}^{Tauc}(E,E_0+\mathrm{W},\quad E_0+\mathrm{W})\quad -I2_{Im}^{Tauc}(E,E_0+\mathrm{W},\quad E_0+3\mathrm{W}/4)]\} \quad (30)$$

where:

$$IC_{Im}^{Tauc}(E,E_r)=\frac{1}{\pi D}\int\frac{\mathrm{d}E_r}{E_r^2[1+[(E_r-E)/D]^2]}=$$
$$-\frac{1}{\pi(D^2+E^2)^2}\left\{(E^2-D^2)\arctan\left(\frac{E-E_r}{D}\right)+D\left[\frac{(D^2+E^2)}{E_r}+E\ln\left(\frac{D^2+(E-E_r)^2}{E_r^2}\right)\right]\right\} \quad (31)$$

$$I2_{Im}^{Tauc}(E,E_0,E_r)=\frac{1}{\pi D}\int\frac{(E_r-E_0)^2\,\mathrm{d}E_r}{E_r^2[1+[(E_r-E)/D]^2]}=$$
$$-\frac{1}{\pi(D^2+E^2)^2}\left\{\left[D^4+E^2(E-E_0)^2+D^2(2E^2-2EE_0-E_0^2)\right]\arctan\left(\frac{E-E_r}{D}\right)\right.$$
$$\left.+DE_0\left[\frac{(D^2+E^2)E_0}{E_r}+(D^2+E^2-EE_0)\ln\left(\frac{E_r^2}{D^2+(E-E_r)^2}\right)\right]\right. \quad (32)$$

Before starting the optimization with the IbridOne method, the function parameters have to be set to initial values good enough to reasonably model $n(\lambda)$. Then, assuming $n(\lambda)$, $k(\lambda)$ values are calculated to perfectly reproduce the $T(\lambda)$ spectrum; from the knowledge of $n(\lambda)$ and $k(\lambda)$, the reflectance spectrum $R_{cal}(\lambda)$ and the merit function $MF=\sum_i(R_{cal}(\lambda_i)-R_{exp}(\lambda_i))^2/\Delta R_i^2$ are calculated. The Levenberg Marquardt non-linear least squares curve fitting (offered by the MINPACK library) is then used to minimize *MF* optimizing some parameters of the coating model (e.g. thickness) and of the analytical functions used to describe $n(\lambda)$. Note that when using IbridOne the transmittance spectrum is always perfectly reproduced by construction.

In order to choose the most appropriate analytical functions to be used in IbridOne, at least in the initial phase, it is advisable to launch the tracking method first, to identify the wavelength-behaviour of a physically meaningful solution subset (see use case #1 and #4 as examples). Otherwise, the choice of oscillator functions should be driven by the physical properties of the material under investigation: in this case the oscillator parameters in the Simulation TAB has to be manually adjusted to obtain a first rough reproduction of the experimental curve before launching IbridOne (see use case #5).

In any case, users should never forget that the reliability of the obtained *n,k* solutions strictly depends on the correctness of the experimental measurements used as input data. We recommend the reading of Appendix B of the user manual which reports some rules of good practice to avoid the most common errors causing artefacts in spectrophotometric measurements.

Prediction of the R and T angular behaviour

Historically, in the first years of its development, kSEMAW was massively used for characterizing architectural glazing: day-lighting and energy consumption evaluation for actual rooms requires knowledge of the luminous and energetic parameters of the fenestration, also at off-normal incidence. The direct experimental measurement of transmittance/reflectance at oblique incidence is very cumbersome: the measurement at a given incidence angle must be separately accomplished for the two light polarizations *s* and *p*; several different angles

must be considered for sampling the angular range of interest, typically [0,90] deg for architectural glazing and [0,60] deg for the case of Concentrated Solar Power (CSP)[23], as well as in Concentrated Photo-Voltaic (CPV).

A simpler approach is offered by the exhaustive optical characterization of the fenestration based on experimental near-normal spectrophotometric measurements and their analysis with a suitable coating optical model. After that, one can numerically evaluate the off-normal incidence behavior[24] of any optical features of the device by means of the tools grouped in the *Simulation* TAB.

Unfortunately, often the multilayer structure of commercial products is undisclosed or it is not perfectly known; therefore further information must be obtained by other techniques[25–27], like neutron spectroscopy and ESCA analysis. Anyway, this reverse-engineering process is very difficult and time-consuming.

On the other hand, when the final purpose is the computing of mean values averaged on a standard spectrum, like the energetic and visible parameters of architectural glazing, these mean values are slightly influenced by the realness of the model: as a matter of fact, even if totally unrealistic, optical models perfectly reproducing the experimental measurements at near-normal incidence allow one to predict off-normal incidence features, averaged on solar or visible spectrum, with good accuracy. By virtue of this fact, the Equivalent Model Algorithm (EMA)[10] has been proposed. The interested reader will find a detailed discussion and a list of the most useful equivalent models in 10; here we just wish to note that kSEMAW is fully EMA-ready.

The situation in CSP and CPV applications is similar but a bit more complex. Mirrors generally work at off-normal incidence to redirect solar radiation on a receiver. As shown in Figure 2 the solar radiation has an intrinsic divergence (the half-angle is about 5 mrad) and the reflected radiation is captured with the acceptance-angle $2\varphi_R$ of the receiver (typically $\varphi_R \leq 20$ mrad). Therefore the reflectance relevant for CSP/CPV can be referred to as *near-specular*, whose value is generally greater than the genuine *specular* reflectance, strictly related to plane-waves.

An international group of experts is drafting the guidelines for reflectance measurement in SolarPACES Task III[3]. Even if in the latest Reflectance Guideline[28] the recommended procedure consists in measuring only the hemispherical reflectance at near-normal incidence, the importance of also measuring near-specular reflectance is now fully acknowledged, but its experimental measurement is a hard task even for highly specialized optics-laboratories because the divergence of the measuring light beam itself may affect the result[29].

Strengthened by the experience gained on glass for building, a more reliable general solution based on a new specific Equivalent Model Algorithm for Solar Mirrors (EMA4SM) was recently presented[30]: EMA4SM

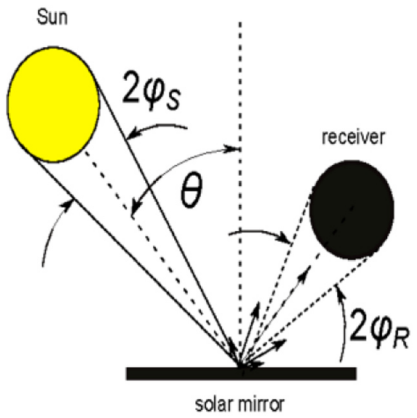


Figure 2. Use case #3: solar mirrors in Concentrated Solar Power (CSP) applications. Θ is the incidence angle; φ_S is the half-angle of solar radiation divergence; φ_R the half acceptance-angle of the receiver.

[3]The international network of researchers and industry experts for the development and marketing of concentrating solar thermal power systems and solar chemistry technologies.

represents the latest evolute adaptation of the Equivalent Model Algorithm (EMA)[10] to the specific case of solar mirrors with the target of predicting the angular behaviour versus incidence and acceptance angle of the solar-weighted reflectance.

The algorithm EMA4SM needs a few experimental data measured at near normal incidence, such as:

1. hemispherical reflectance spectrum measured in the solar range (320–2500 nm);
2. near-specular or conic reflectance measured at single wavelength and several different acceptance angles in the range of interest.

Considering the high specialization of both the model and the single wavelength experimental measurements, we have decided to separate this functionality from kSEMAW and arrange the new software SMQexpo for dealing the specific case of solar mirrors. Such software embraces the Open Source philosophy and is freely distributed; interested people can request it by sending an email to `marco.montecchi@enea.it`.

Therefore actually kSEMAW can be only used for highly specular solar mirrors, i.e. in the cases where near-specular reflectance is equal to the specular one, within the experimental error.

Implementation and operation

Referring to the user manual for more details, here we just note that beside the installation of kSEMAW on PC with Linux operative system (Manjaro or Debian distro), now the installation under MS Windows is also described. Furthemore, to make life easier, we even provide the MS Windows executable.

To avoid any confusion with versions older than 1.0.0, the executable (both in Linux and MS Windows) is now named `ksemawc`.

`kSEMAWc` needs the following main libraries:

1. Qt, for the Graphical User Interface (GUI)
2. Qwt, to generate the plots
3. C/C++ MINPACK, for Levenberg-Marquardt non-linear least square routine

When launched, two windows pop-up: the GUI and a terminal; the latter shows the progress of the workflow with some auxiliary messages.

The GUI, shown in Figure 3, is composed by a top part, structured in 6 “tabs”, ordered in logical sequence, and a bottom part, always visible.

The 6 TABs are:

1. **Valin:** selection of *nk*-files and experimental measurements to be imported in the analysis work bench.
2. **Model:** setting of the optical device model.
3. **Simulation:** simulation of measurements on the basis of known (n, k).
4. **Numerical search:** : Exhaustive Numerical Search of (n_λ, k_λ) solutions in the spaces (λ, n) and (λ, k).
5. **Data Fit:** with the following functionalities:
   - Fit nk-data
   - Fit dielectric constant data
   - Fit experimental spectra
   - Fit with the IbridOne procedure
6. **Graph range:** management of XY plots

The bottom part, always visible, contains

- loading/saving the SEMAW project file (`.Spj`)
- loading a *nk*-file to be shown in the plots

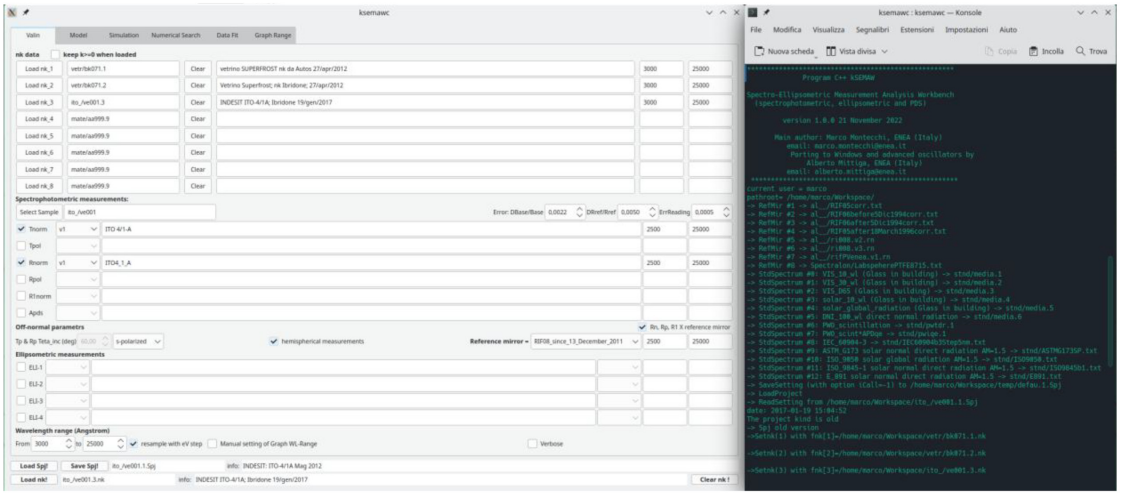


Figure 3. Graphical interface and terminal of kSEMAW.

Use cases

The complete file-kit of each one of the five use cases presented here are included in the working directories; path and file name are given in each example. Please see *Underlying data*.

Use case #1: substrate

The evaluation of the complex refractive index of a bare substrate is the simplest case for testing kSEMAW, but at the same time it is a very important task: the most common error in characterizing thin film devices is to neglect the preliminary characterization of the substrate. As a matter of fact, although for a given type of material the real part of the refractive index is fairly constant over different specimens, and well compatible with the values reported in literature, the same cannot be said for the extinction coefficient: in the nearness of absorption tails, such as the UV transmittance cutoff for glass and quartz, the user should not be surprised to find differences much greater than the measurement error, even among substrates belonging to the same batch of supply! Thus if one intends to analyse a series of samples, the preliminary check about the homogeneity of the available substrates and, if necessary, the selection of a group with the same features, are mandatory. In order to properly characterize thin film specimens, one should take care of loading the right *nk*-file of the substrate in the *Valin* TAB, otherwise the found solutions will suffer from more or less evident artefacts.

The use case here presented consists of a fused silica, 2.0 mm thick, summarized in the kSEMAW project `quar/bk026.2.Spj`.

As soon as the project is loaded, the experimental transmittance and reflectance spectra related to the specimen here considered, coded as `quar/bk026`, are listed in the *Valin* TAB; they were measured with a Perkin Elmer Lambda 900 equipped with a 15 cm integrating sphere in the wavelength range 3000–25000 Å. The reflectance file is not yet normalized to the reference mirror; kSEMAW can do it when "*Rn Rp R1 for" is checked and the proper mirror is selected among the list; please note that the list of reference mirrors can be easily customized following the instruction reported in the user manual.

In general, once *nk*-files and measurements are set, kSEMAW computes the maximum common wavelength range where data of all selected inputs are available. By default, that is the range used for re-sampling both

nk-file and experimental measurements on a common base of 201 points[4], with step in wavelength (Å) or in energy (eV) if the checkbox "resample with eV step" is checked. The latter choice, selected in the current case, is recommended for thin film coatings because it allows to view the interference fringes with an almost regular period.

The model is controlled by the GUI in the *Model* TAB: the actual specimen consists of a single layer, "bulk" type: i.e. e.m. wave propagation is treated by neglecting interference among the several contributions coming from the two interfaces; that is certainly true for the light beam of any UV-VIS-NIR spectrophotometer. The layer thickness is here set to 2.0 mm, that is the experimental value measured with a caliper.

As a general rule it is preferable to start with the Exhaustive Numerical Search method because it does not need the modelling of $n(\lambda)$. This method is controlled by the GUI in the *Numerical-search* TAB, except for the *n*-range of search which coincides with the one used in the plots, settable in *Graph-Range* TAB.

At the beginning of the study of a new material, or simply for checking the suitability of the chosen couple of measures to find solutions, the user can launch the search of solutions in the (n, k) space by pushing the button "Search in n-k space @"; here the considered wavelength is the one specified to the right of this button (the user can set λ_{min}, λ_{max} or another wavelength in the range). As an example Figure 4 shows the search at λ = 3100 Å. In that graph two lines are drawn for each measurement: in this case two blue lines for T and two green lines for R. Each couple of lines limit the belt in which (n_λ, k_λ) allow to reproduce the experimental values within the error; if the error was null, the belt would collapse to a single line. The intersection area between (n_λ, k_λ) belts from different measurements represents the common solution area. Here the solution is (n = 1.485, $k = 5\ E - 08$).

Once the *n*-range of search is set, the Exhaustive Numerical Search method starts by pressing the dedicated button; Figure 5 shows the results: in the first row, the black vertical bars represent the Transmittance and Reflectance spectra with their errors (see the *Valin* TAB in the user manual). In the second row the black vertical bars represent the computed complex refractive index.

The other computational method, IbridOne, requires the preliminary modelling of $n(\lambda)$ with appropriate analytical functions which can be set in the *Simulation* TAB. In the actual case we consider the fit-option composed by: 1) Direct-Gap Tauc oscillator peaked at 7 eV; 2) Drude term; 3) Flat term. The first term is used to model the growth of n towards UV; the second one for modelling its reduction towards IR; the flat term represents

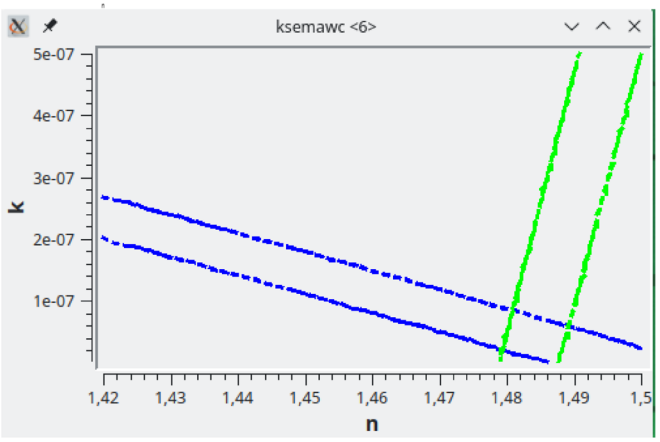


Figure 4. Use case #1: graphical solution search in the complex refractive index (*n*, *k*) space. The crossing between the two solution-belts of Transmittance (blue) and Reflectance (green) represents their common solution at λ =3100 Å.

[4]That value was set in the early days of software development in '90, on a workstation HP 9000 equipped with a 100 px wide terminal! Later we continued to keep that value because it does not slow down the solution computing in the selected wavelength range, but it ensures a sufficient sampling-density to represent a spectrum with many interference fringes, provided the step is set to energy.

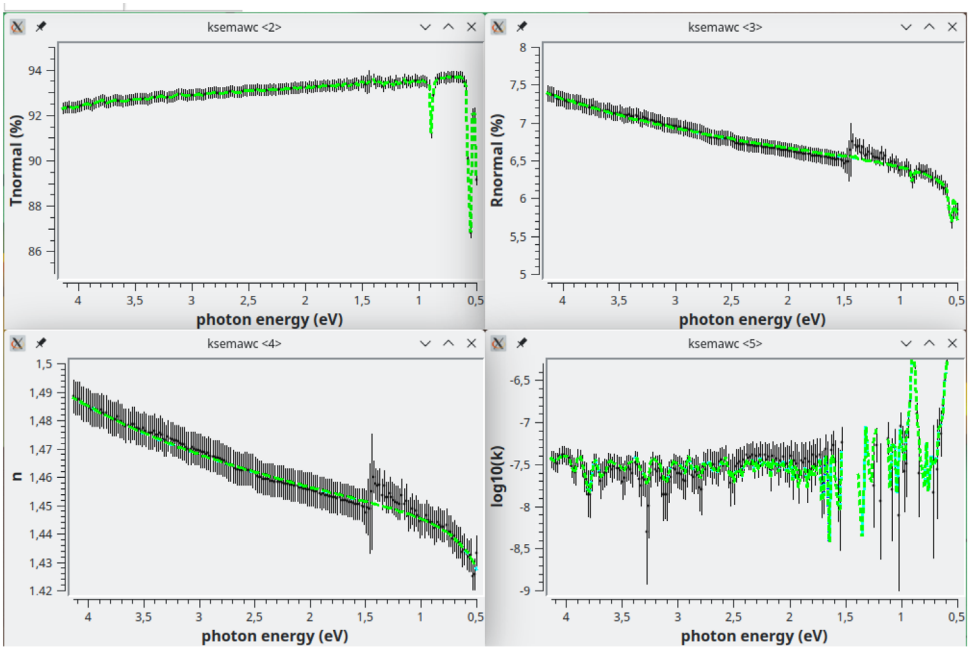


Figure 5. Use case #1: Transmittance (top-left) Reflectance (top-right), refractive index (bottom-left) and extinction coefficient (bottom-right) of fused silica `quar/bk026`. In the bottom row the black vertical bars represent the solutions obtained by the Exhaustive Numerical Search method. In each one of the four graphs the green solid lines represent the solutions obtained by the IbridOne method.

the vacuum (see Equation 1) plus the global effect of oscillators with peak energy far from the considered energy range.

Once a suitable fit-option is set, one should surf to the *Data Fit* TAB, which controls the IbridOne computational method. Here one can compose a list of the parameters he wants to consider, and each one of them can be enabled or excluded from the best fit procedure.

The IbridOne procedure runs by pushing the button "Best Fit with IbridOne!"; the new solutions are here plotted as green-dashed lines in Figure 5. With respect to the solutions obtained by the Exhaustive Numerial Search, now the behavior of $n(\lambda)$ is totally smooth because it is computed by the analytical functions composing the fit-option; in such a way the reflectance step occurring at about 860 nm, caused by the detector change in the spectrophotometer, has no effect on $n(\lambda)$. Conversely the $k(\lambda)$ solutions obtained with the two methods are almost identical.

Please note that by definition IbridOne allows the perfect fitting of the transmittance spectrum.

Use case #2: twin AR coating on glass

The next example was chosen among the several specimens analysed along the optimization of the sol-gel dipping process of porous silica with the aim to obtain solar AR coatings for the glass used to wrap the steel receiver tubes of parabolic trough solar collectors; this process is expected to produce symmetrical twin AR-films on the two sides of the substrate.

The specimen here considered is coded as `sipo/ve096;` although its features are far from the goal, the case is very useful for learning kSEMAW.

Let us start by loading the initial project `sipo/ve096.0.Spj`. The *nk*-file of the substrate is set at the top of the *Valin* TAB (`vetr/bk048.5`); its thickness is 3.3 mm. In the same TAB, experimental Transmittance and Reflectance are set. The common maximum wavelength range is 3000–25000 Å. It is a good practice to

start the *nk*-solution search by considering the simplest model. This approach is used in the initial project `sipo/ve096.0.Spj` and therefore in the *Model* TAB the user will find a model composed by a twin symmetrical single homogeneous film on both sides of the substrate. The film thickness is set to 1875 Å.

The Exhaustive Numerical Search method is controlled by the GUI in the *Numerical-Search* TAB. As already discussed in use case #1, the first step is the delimitation of the n-range of search. By trial and error, [1.2,1.6] is found to be fine.

The Exhaustive Numerical Search method is launched when the dedicated button is pressed. The results are shown in Figure 6: the *n*-solutions are not connected at the "crossings" related to the extremes $\lambda_m = 4nd/m$ corresponding to $m = 2$ ($E \approx 2.5$ eV) and $m = 3$ ($E \approx 2.9$); please note that in the case of odd extremes, the related crossings are shifted at lower energy[12].

As explained in the papers[12,13], thickness and inhomogeneity of the film can be determined by optimizing the connection of such crossings. To this purpose one should properly modify the film parameters in *Model* TAB, relaunch the Exhaustive Numerical Search, and observe the effect on the solution crossings related to $m = 2$ and $m = 3$: in the actual case one can easily verify, by trial and error, that the solutions are well connected when thickness and linear *n*-gradient are in the range [1865,1890] Å and [-0.0040,-0.0120], respectively.

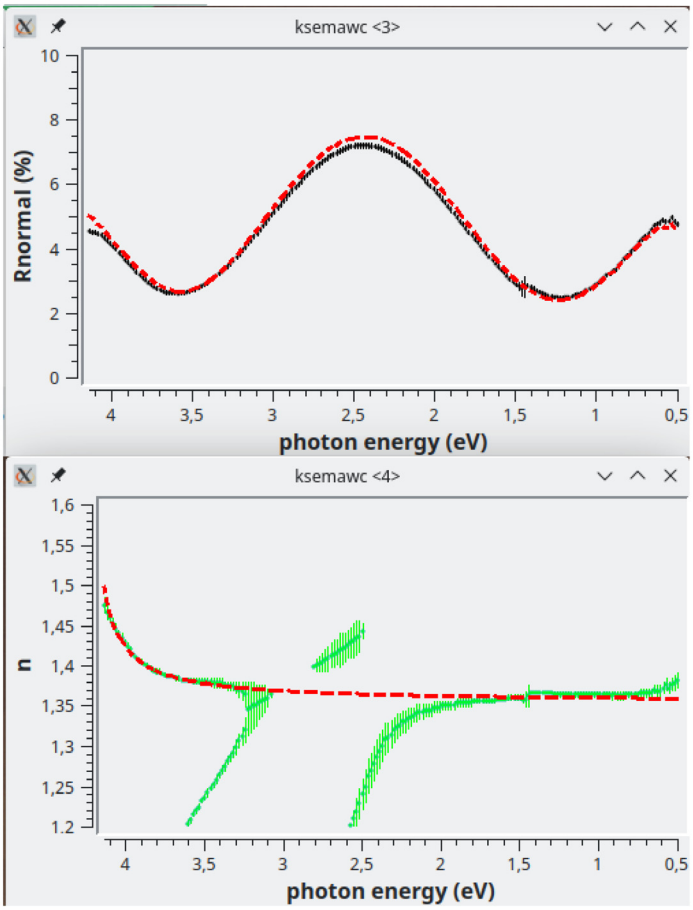


Figure 6. Use case #2: Reflectance (top) and *n*-solutions obtained by the Exhaustive Numerical Search method (bottom) of the AR coating `sipo/ve096` by assuming two twin homogeneous films, 1875 Å thick, on the two sides of the substrate. The red dashed line in the top graph is the reflectance computed with the analytical $n(\lambda)$ (red dashed line in the bottom graph) composed by two quantum homogeneous oscillators and one flat term (see text).

After this first important adjustment, the model parameters can be automatically refined by means of another computing method offered by kSEMAW: the IbridOne algorithm. This method requires the preliminary modelling of $n(\lambda)$ with some proper analytical functions, among the several ones offered in the *Simulation* TAB; there one can set the parameters and verify the agreement with the computed n-solutions by pushing "Simulate !". In the current case, the part of the achieved solutions having physical meaning are fairly well fitted with the sum of 3 terms: 1) a quantum-homogeneous oscillator peaked at 5 eV; 2) a quantum-homogeneous oscillator peaked at 4.25 eV; 3) a Flat term. The roughly adjusted function is drawn as a red dashed line in the bottom graph of Figure 6; the simulated reflectance computed with this function is drawn as a red dashed line in the top graph.

With these premises, in the "IdridOne" TAB one can set the list of parameters to be viewed and select those to enable for the best-fitting. We found satisfactory results by enabling: thickness, n-gradient, and the amplitude C parameter of each one of the three terms used to model $n(\lambda)$. The final results are saved in the project `sipo/ve096.2.Spj` and shown in Figure 7. The optimized film thickness is 1876 Å and the n-gradient is linear along the film thickness with a negative value (from the substrate to air) of -0.0084 (normalized value; see the user manual). Transmittance and Reflectance perfectly agree with the computed spectra; the continuous lines in n and k graphs represent the solutions obtained by IbridOne, while the green vertical bars are the solutions computed by the Exhaustive Numerical Search method once the model was optimized by IbridOne; now the n-solution crossings are perfectly connected.

Another very interesting point to discuss is the mild negativity of k for $\lambda > 860nm$ ($E < 1.44$eV): this artefact is due to the imperfect characterization of the substrate which is just a bit less absorbing then the specimen used for determining the substrate refractive index. As a matter of fact by reducing the substrate thickness to 2.5 mm the artefact almost disappears.

Use case #3: solar mirror

Here we just consider the simple case of a glass-based highly-specular mirror, coded as `ag__/ve010`: it consists of a silver layer deposited on a glass substrate 0.95 mm thick; the silver side interfaced with the air is protected with a specific protective treatment ensuring more than 10 years of lifetime in outdoor conditions. Therefore the specimen is specular just only on the glass side, i.e. it is a so-called "second surface mirror".

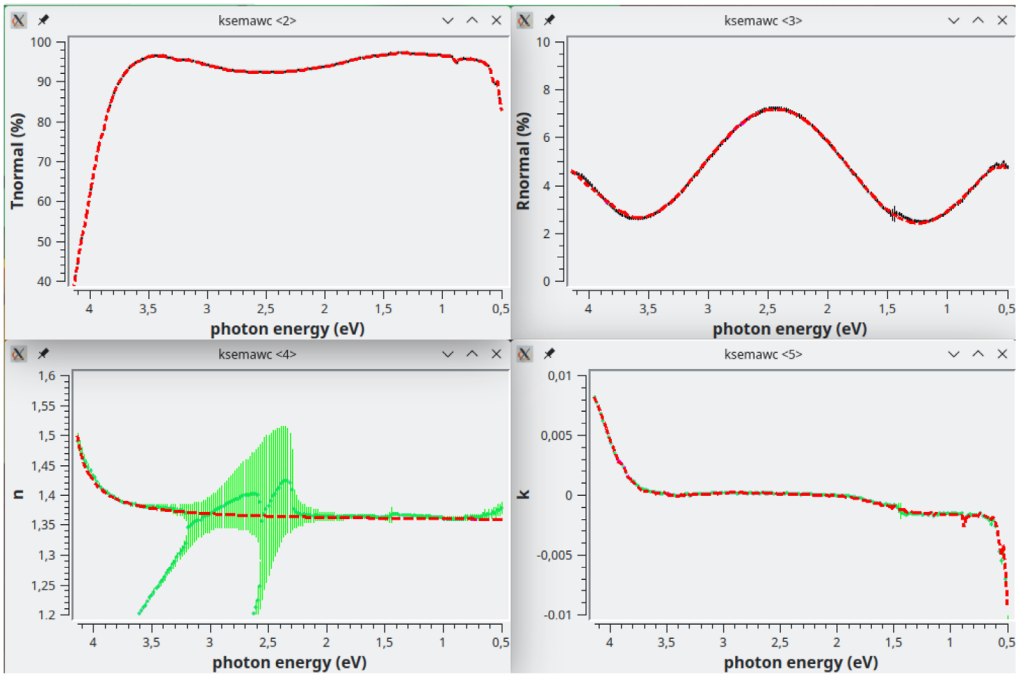


Figure 7. Use case #2: results obtained with the refined optical model (see text). Transmittance (top-left) Reflectance (top-right), refractive index (bottom-left) and extinction coefficient (bottom-right) of twin AR coating on glass.

Since scattering is very low, its features for CSP applications can be simply obtained by the angular behaviour of the solar-weighted specular (back) reflectance, which can be evaluated on the basis of the optical characterization shown in the following.

Let us consider the project `ag__/ve010.6.Spj`. As usual, the *nk*-file of the substrate is set at the top of the *Valin* TAB (`vetr/bk067.2.nk`); the complex refractive index of Silver reported in the literature[31] `ag__/bk000.9.nk` and its customization on the actual sample `ag__/ve010.6.nk` are also set. The back-reflectance (*R*1) `ag__/ve010.v2.r1` is the experimental spectrum used for the characterization.

In the *Model* TAB the simplest model is already set: a single homogeneous film of silver, thick enough to suppress transmittance (5000 Å), on a glass substrate 0.95 mm thick, with complex refractive index `vetr/bk067.2.nk`.

In the *Simulation* TAB the *nk*-unknown is set to the Ag literature file. By pressing "Simulate!", Reflectance *n* and *k* simulated-spectra are drawn in the plots; the reflectance is only approximatively reproduced.

To calculate better *nk* solutions the user has to surf to *Numerical Search* TAB. As a general rule only one of the two unknowns *n* and *k* can be evaluated when just a single experimental spectrum is available; in that case, by default, the Exhaustive Numerical Search evaluates *k* while *n* is set to the value referring to the simulation option already selected in Simulation TAB. The achieved solution are shown in the first row of Figure 8; the calculated *R*1 spectrum (bottom-left) now perfectly agree with the experimental one.

The solar-weighted reflectance versus incidence angle shown at the bottom-right of Figure 8 was computed by setting the "Average type" combo-box (in *Simulation* TAB) to solar spectrum ASTM G173, and pushing the button "Plot <T>, <R>, <R1> vs theta !"; in the graph, reflectance and back-reflectance are plotted in cyan and green, respectively; the latter is the one of our interest; the average value at normal incidence is displayed in this TAB for both experimental (95.22%) and simulated (95.35%) reflectance; the solar-weighted reflectance increases with the incidence angle.

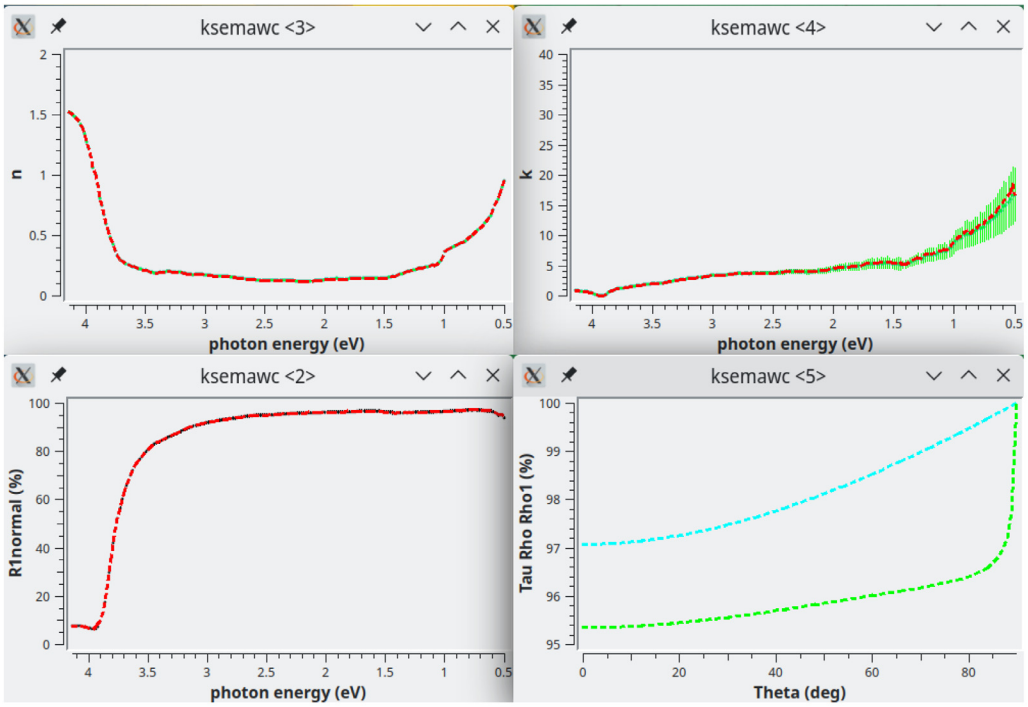


Figure 8. Use case #3: Solarlux mirror `ag__/ve010`: on top-left, literature values of silver refractive index[31]; on top-right, extinction coefficient obtained by the Exhaustive Numerical Search method. Bottom-left, experimental (black dot & bars) and calculated (red dashed-line) back-reflectance; bottom-right, solar-weighted (ASTM-G173) front (cyan) and back (green) reflectance versus incidence angle.

The angular behaviour of the solar-weighted reflectance is a very important information for predicting the mirror effectiveness when used to make the concentrators of a specific solar plant. That is a way for comparing the performances of different commercial solar mirrors in a specific application.

Use case #4: Transparent conductive oxide (IWO)

Transparent conductive oxides (TCO) play an important role in the photovoltaic technology. They are deposited as top layers on heterojunction solar cells and they serve both as antireflective coatings to reduce optical losses and as conductive layers to collect the photogenerated carriers[32,33]. Among TCOs, tungsten-doped indium oxide (IWO) is recently attracting much attention[34]. IWO films are characterized by a wide energy gap >3.5 eV, high transparency in the UV-VIS spectral range and the presence of some absorption in the NIR, related to the density of free electrons in the material.

The specimen here considered is an IWO sample grown by radio frequency reactive sputtering; the kSEMAW project is `iwo/IWO_069.1.Spj`.

The substrate is fused-silica, 1 mm thick; the related *nk*-file is `vetr/SLG_sigmaAldrich.1.nk`. Transmittance and Reflectance were measured with a Perkin Elemer L950 spectrophotometer equipped with a 15 cm integrating sphere; in this case the reflectance file is already normalized to the reference mirror thus in *Valin* the checkbox "*Rn Rp R1 for" is unchecked.

The common maximum wavelength range is 2500-25000 Å, but the UV limit of the range set in *Valin* must be increased to 2700 Å because at shorter λ the transmittance value is zero (within the experimental error) making it useless for evaluating *k*.

The simplest model consists of a homogeneous film on the substrate. On the basis of the deposition duration and the film growth-rate, the film thickness is expected to be about 93 nm.

Under these assumptions one can launch the Exhaustive Numerical Search method and use the crossing points of the *n*-solutions to improve the model, as already discussed in use case #2.

The examined wavelength range includes m = 2, 3, 4 crossings: the even ones are well connected, confirming the hypothesis of film homogeneity, while m = 3 suffer from thickness underestimation. This crossing point becomes connected by increasing the thickness to about 1010 Å.

From this point on one can take advantage of the IbridOne method. To that purpose the *n*-solutions having physical meaning must be modelled by analytical functions; a good option is to consider the three terms: Direct-Gap-Cody, Flat, and Drude. The first (third) term models the absorption in UV-blue (NIR) range.

We run IbridOne several times, gradually refining the parameters, among which the film thickness definitively set to 1014 Å. Figure 9 shows the optimized results: Transmittance and Reflectance experimental spectra are in perfect agreement with the calculated ones on the basis of the complex refractive index shown in the middle row as red dashed line. As usual, the green vertical bars represent the solutions obtained by the Exhaustive Numerical Search method.

The *n*-plot here is very instructive because it makes clear that part of the solutions obtained with the Exhaustive Numerical Search method are merely mathematical ones; the physical solutions are the ones closer to the red dashed line; the others should be manually deleted by activating the polygonal area selection with the button "Select n-solutions!".

It has to be noted that kSEMAW gives the possibility to display also the real and imaginary parts of the dielectric constant (see for example the bottom rows in Figure 9) when, in the *Simulation* TAB, the related checkbox is enabled. This is a very useful feature when working on semiconductor materials with extended and structured absorption bands because such a plot can help to configure a suitable oscillators set by comparison with literature data or with a previous fit.

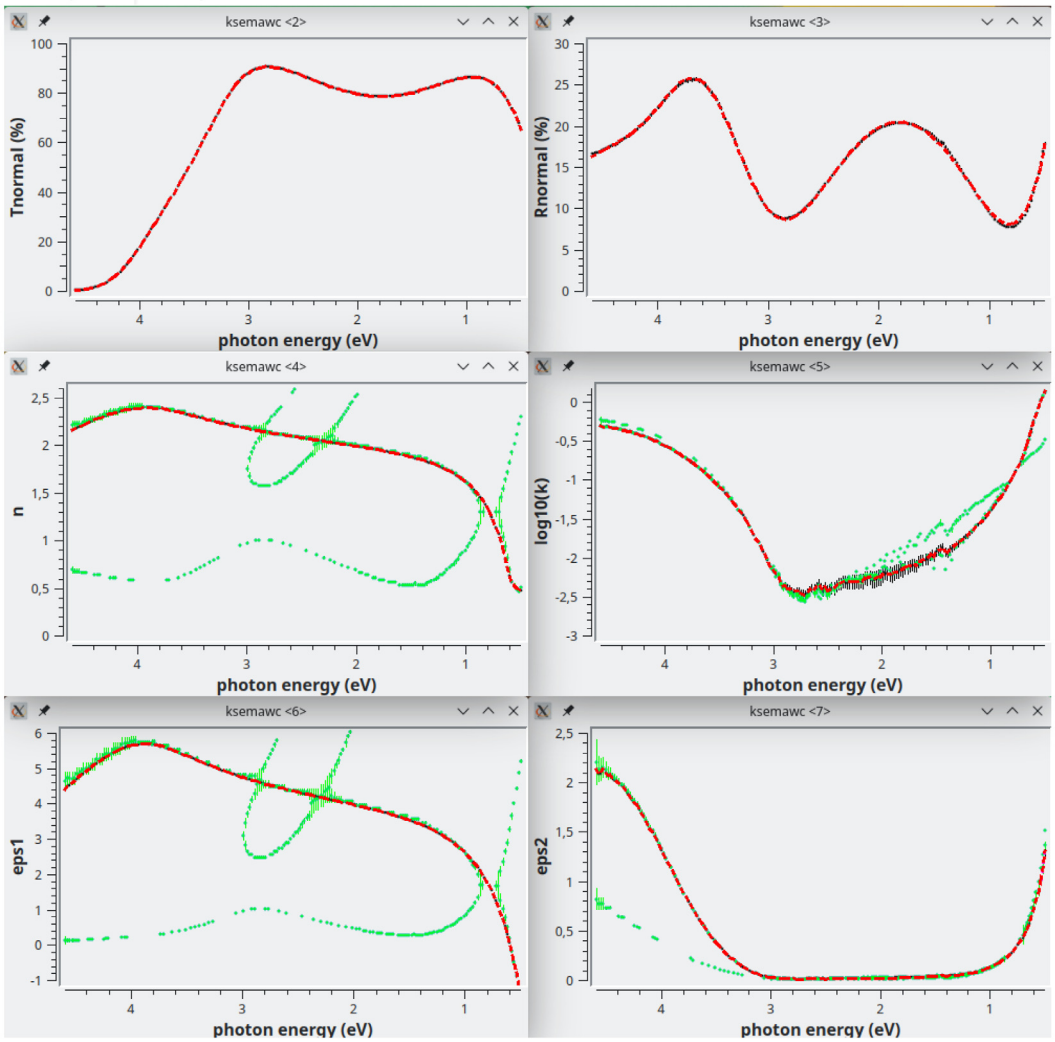


Figure 9. Use case #4: Transmittance (top-left), Reflectance (top-right), refractive index (centre-left), extinction coefficient (centre-right), ϵ_1 (bottom-left) and ϵ_2 (bottom-right) of `iwo/IWO_069`. The green vertical bars represent the solutions obtained by the Exhaustive Numerical Search method while the red dashed lines represent the solutions obtained by the IbridOne method.

Use case #5: transition metal dichalcogenide (MoS_2)

The development of several kinds of new photovoltaic devices would greatly benefit from the availability of a semi-transparent hole transport material (HTM) with a high work function[35]. MoS_2 is a good candidate for this role since it has an indirect optical gap at 1.17–1.23 eV[36] while the first direct gap is at 1.85 eV[37]. The indirect gap gives a rather weak absorption so that films with a thickness of a few tens of nanometers are quite transparent for wavelengths greater than 800 nm. MoS_2 photothreshold (i.e. the energy difference between the vacuum level and the valence band maximum) is quite high being about 5.6 eV[38], so that a p-type doped MoS_2 would show a work function larger than 5 eV, suitable for HTM applications. MoS_2 was already employed in a monolithic CZTS/Si tandem device where a MoS_2/FTO/ZnO multilayer structure was used as intermediate contact[39] between the top and bottom cells. The MoS_2 layer used in this multilayer was obtained by metallic Mo sulfurization, as the sample considered in the example below.

The specimen here considered is a film, about 90 nm thick, deposited on a borosilicate Corning glass, 1.1 mm thick with *nk*-file `vetr/bk082.1.nk`; the specimen is coded as `mos2/MoS2_279_BSG`. Transmittance and Reflectance spectra were recorded in the UV-VIS-NIR (2500-25000 A) spectral range as described in the use case #4 and, as before, the UV limit of the range set in the *Valin* TAB must be increased to 2900 Å to exclude the data region with almost zero transmittance (unusable to evaluate *k*).

For educational purposes we arranged the initial project `mos2/MoS2_279_BSG.paper.9.Spj` to show how to set-up, on the basis of experimental and literature data[36], a suitable oscillator assortment for modelling the dielectric constant.

As a first reasonable option, based on the known material properties,a set of 5 analytical functions was initially considered in the *Simulation* TAB, including: i) an Indirect-gap and a Direct-Gap-Cody terms at about 1.2 and 1.8 eV respectively, corresponding to the indirect and direct gap energy values, ii) other two Direct-Gap-Cody terms to describe the absorption at higher energies and iii) a constant (Flat) term. From the same TAB, both T and R spectra were calculated and compared with the experimental data: the indirect absorption in the material is so weak that the indirect-gap term was found to have negligible effect in the simulation of optical data and therefore it was removed from the oscillator model.

After a few manual adjustments, we got the option Fit #1 detailed in Figure 10, giving a fairly good reproduction of all the main features of the experimental spectra, thus validating the proposed oscillator model and its physical meaning. Simulation results are shown in Figure 11. At this point , thickness and *n*-gradient of

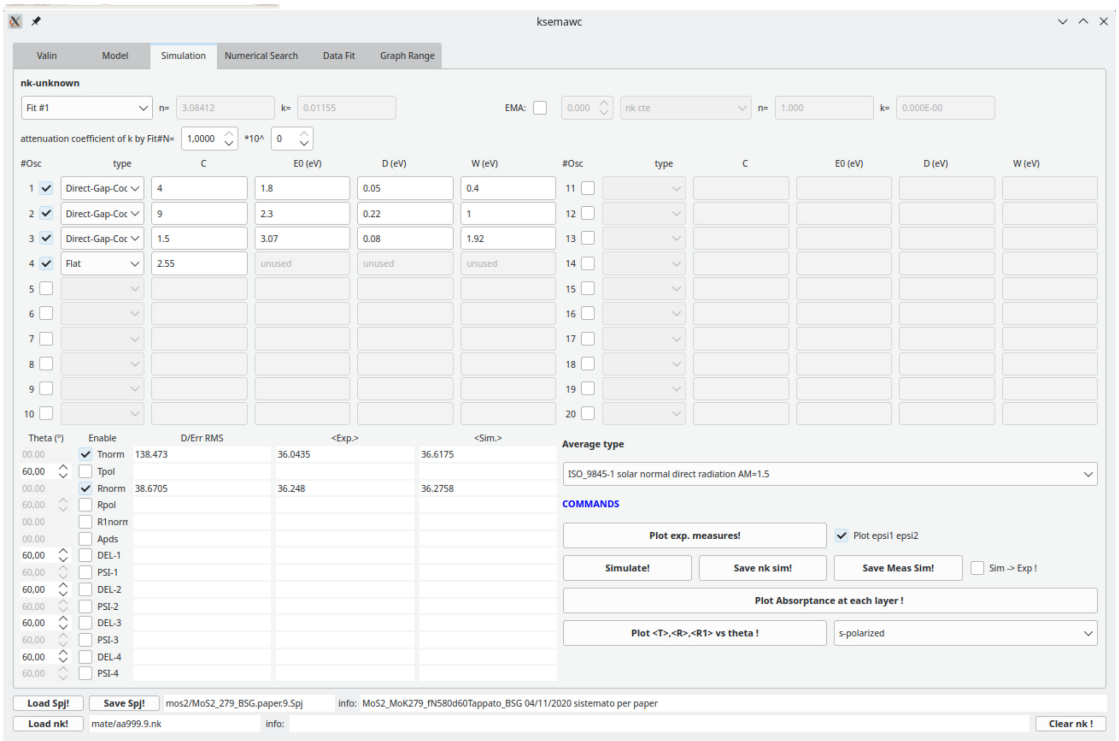


Figure 10. Use case #5: *Simulation* TAB with initial oscillator assortment for modelling the dielectric constant of a MoS_2 film on the basis of literature data. Parameters *C* (oscillator amplitude) and *W* (band width) were roughly manually adjusted for improving the agreement of the computed spectra with experimental Transmittance and Reflectance shown in Figure 11.

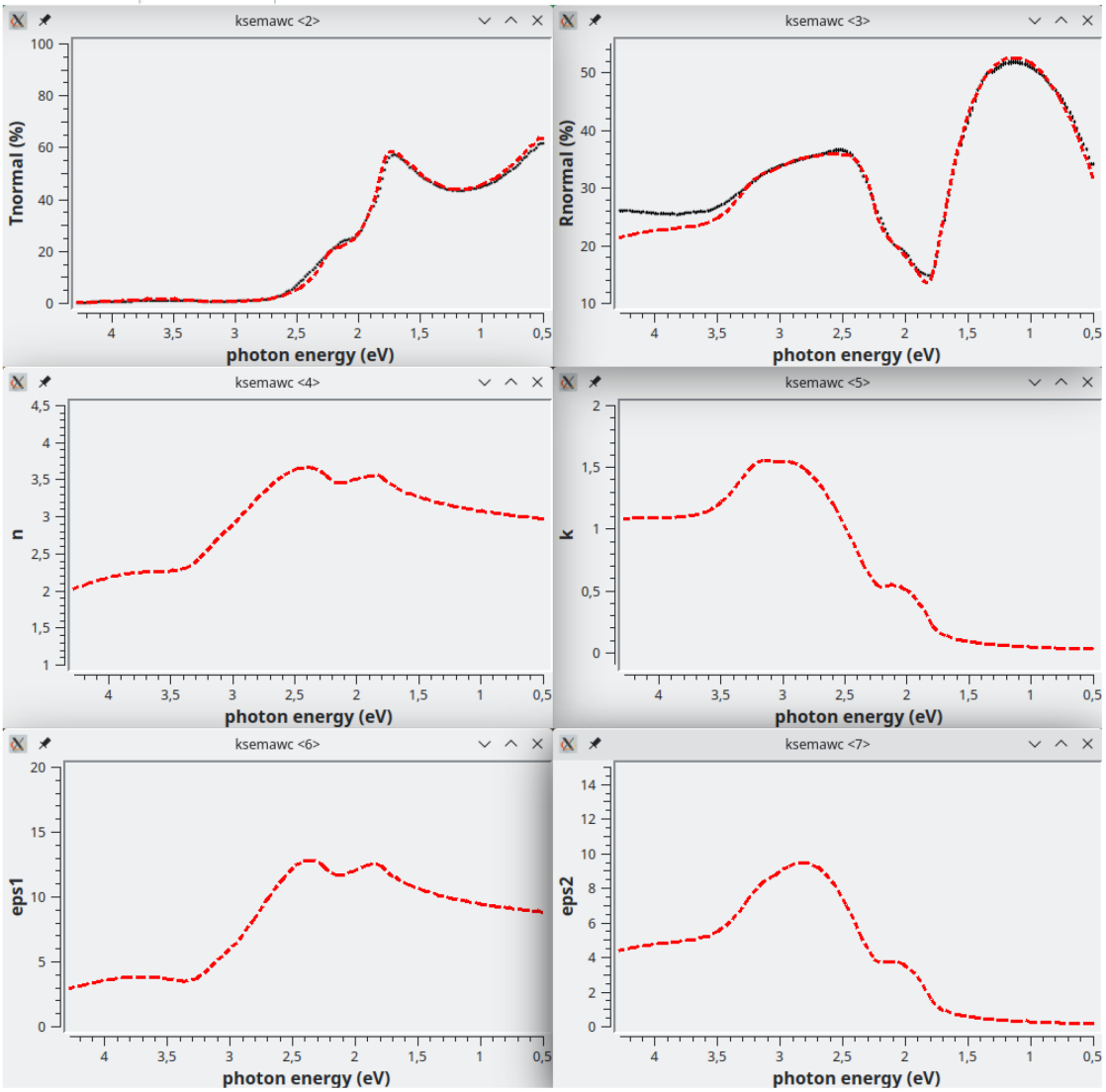


Figure 11. Use case #5, initial situation: Transmittance (top-left), Reflectance (top-right), refractive index (centre-left), extinction coefficient (centre-right), permittivity real part ϵ_1 (bottom-left) and permittivity imaginary part ϵ_2 (bottom-right) of `mos2/MoS2_279_BSG`. The simulated curves, reported as red dash line, were calculated with the oscillator assortment shown in Figure 10.

the film, as well as the *C* parameters of the 4 oscillators composing Fit#1 were further refined by means of the IbridOne method; we found it not useful to enable the others parameters in the best-fitting procedure since a satisfactory agreement between the experimental and fitted curves is obtained. The optimized results are summarized in Figure 12, Figure 13. As previously explained, the calculated transmittance is always perfectly reproduced by construction using the IbridOne method. The final project was saved as `mos2/MoS2_279_BSG.1.Spj`.

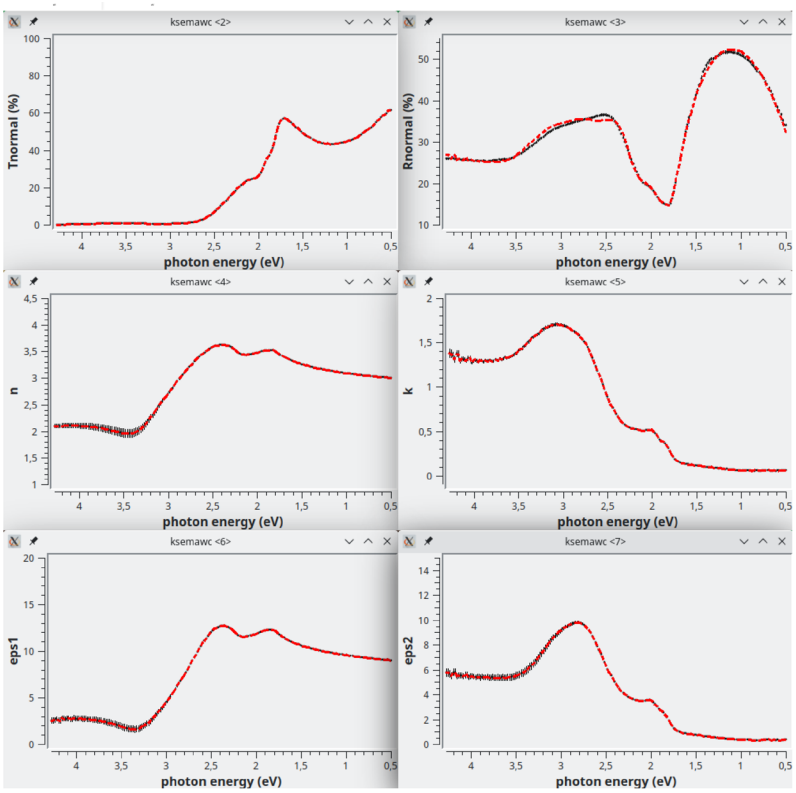


Figure 12. Use case #5, after optimization by the IbridOne method: Transmittance (top-left), Reflectance (top-right), refractive index (centre-left), extinction coefficient (centre-right), ϵ_1 (bottom-left) and ϵ_2 (bottom-right) of mos2/MoS2_279_BSG. The red dashe lines represent the solutions obtained by the IbridOne method and the black vertical bars their error.

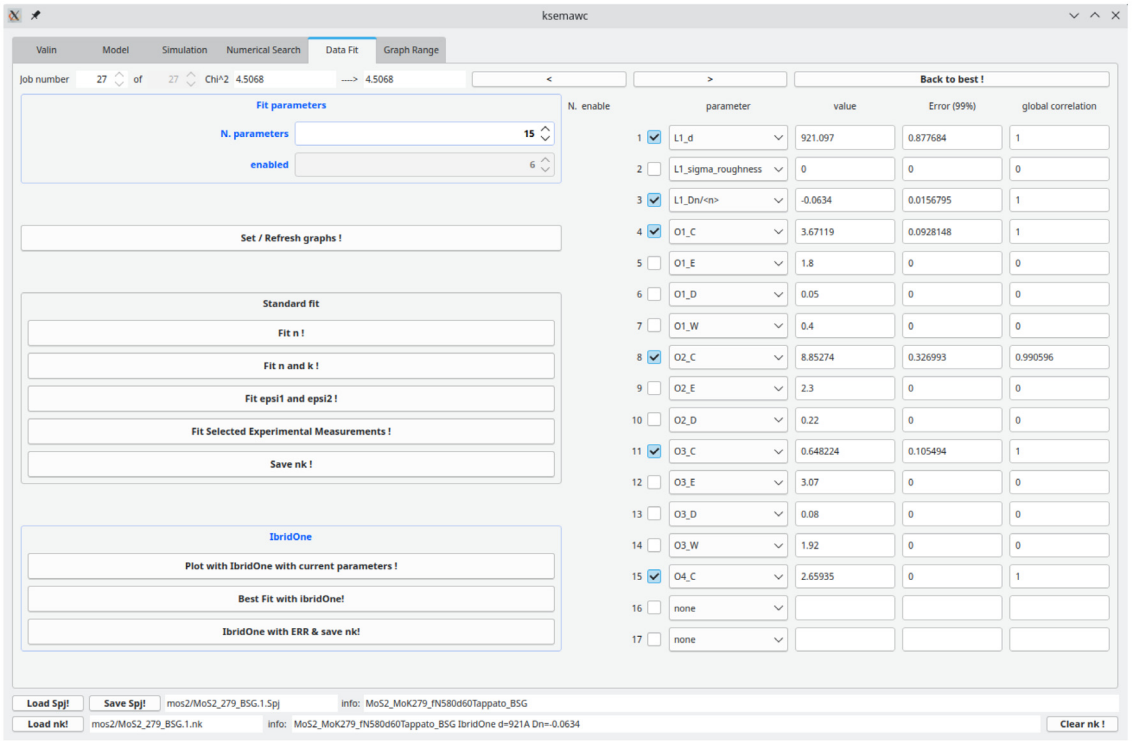


Figure 13. Use case #5: *IbridOne* TAB with the optimized parameters.

Data availability

Underlying data

Zenodo: mmonty1960/ksemaw: v1.0.0. http://doi.org/10.5281/zenodo.7398317[14].

This project contains the following underlying data:

- underlying data for use case 1, coded as `quar/bk026`
- underlying data for use case 2, coded as `sipo/ve096`
- underlying data for use case 3, coded as `ag__/ve010`
- underlying data for use case 4, coded as `iwo/IWO_069`
- underlying data for use case 5, coded as `mos2/MoS2_279_BSG`,
- manuale_ksemawc_v1.0.0.pdf (user manual)

Data are available under the terms of the GNU Affero General Public License version 3.

Software availability

Source code available from: https://github.com/mmonty1960/ksemaw

Archived source code at time of publication: http://doi.org/10.5281/zenodo.7398317[14]

License: GNU Affero General Public License version 3

Acknowledgements

Many thanks to:

- Francesco Biccari for his useful suggestions for simplifying the software distribution
- Luca Serenelli for his support for outlining the installation procedure
- Enrico Nichelatti for the wise help in the search for analytical solutions of the integrals on the density of the states, as well as for the LaTeX adaptation of the manual

References

1. Wasa K, Kitabatake M, Adachi H: **1-thin film materials and devices**. In: Kiyotaka Wasa, Makoto Kitabatake, and Hideaki Adachi, editors, *Thin Film Materials Technology.* William Andrew Publishing, Norwich, NY, 2004; 1–16.
Publisher Full Text
2. Macleod HA: **Thin-Film Optical Filters**. Macmillan Publishing Company, 1986.
Reference Source
3. Masetti E, Montecchi M, da Silva MP: **Analysis of the oxidation of polycrystalline zinc selenide by spectroscopic ellipsometry and photothermal deflection spectroscopy.** *Thin Solid Films.* 1993; **234**(1–2): 557–560.
Publisher Full Text
4. Polato P, Franz H, Rustichelli F, *et al.*: **Characterization of TiN_xO_y thin films on architectural glass by x-ray reflection and spectrophotometry.** *Thin Solid Films.* 1994; **248**(2): 184–192.
Publisher Full Text
5. Baccaro S, Barone LM, Borgia B, *et al.*: **Ordinary and extraordinary complex refractive index of the lead tungstate ($PbWO_4$) crystal.** *Nuclear Instruments and Methods in Physics Research Section A: Accelerators, Spectrometers, Detectors and Associated Equipment.* 1997; **385**(2): 209–214.
Publisher Full Text
6. Montecchi M, Ingram Q: **Study of some optical glues for the compact muon solenoid at the large hadron collider of cern.** *Nuclear Instruments and Methods in Physics Research Section A: Accelerators, Spectrometers, Detectors and Associated Equipment.* 2001; **465**(2–3): 329–345.
Publisher Full Text
7. Deiters K, Diemoz M, Godinovic N, *et al.*: **Investigation of the avalanche photodiodes for the cms electromagnetic calorimeter operated at high gain.** *Nuclear Instruments and Methods in Physics Research Section A: Accelerators, Spectrometers, Detectors and Associated Equipment.* 2001; **461**(1–3): 574–576.
Publisher Full Text
8. The CMS Collaboration, Chatrchyan S, Hmayakyan G, *et al.*: **The CMS experiment at the CERN LHC.** *JINST.* 2008; **3**: S08004.
Publisher Full Text
9. Montecchi M: **Approximated method for modelling hemispherical reflectance and evaluating near-specular reflectance of csp mirrors.** *Sol Energy.* 2013; **92**: 280–287.
Publisher Full Text
10. Montecchi M, Nichelatti E, Polato P: **Hybrid equivalent model algorithm or the prediction of glazing angular properties.** *Sol Energy Mater Sol Cells.* 2002; **71**(3): 327–342.
Publisher Full Text
11. Nichelatti E, Montecchi M, Montereali RM: **Optical reflectance and transmittance of a multilayer coating affected by**

refractive-index inhomogeneity, interface roughness, and thickness wedge. *J Non-Cryst Solids.* 2009; **355**(18–21): 1115–1118.
Publisher Full Text

12. Montecchi M, Masetti E, Emiliani G: **Thickness and model optimization in characterization of optical interference films by using discontinuities of *n*(λ)solutions.** *Pure Appl Opt.* 1995; **4**: 15–26.
Publisher Full Text

13. Montecchi M: **Characterization of inhomogeneous optical interference films using a complex parabolic profile model.** *Pure Appl Opt.* 1995; **4**: 831–839.
Publisher Full Text

14. mmonty1960: **mmonty1960/ksemaw: v1.0.0 (Version ksemaw).** *Zenodo.* 2021.
http://www.doi.org/10.5281/zenodo.7398317

15. Born M, Wolf E: **Principles of Optics**. Pergamon Press, Oxford, 6th edition, 1987.

16. Yariv A: **Quantum Electronics**. John Wiley & Sons, 2nd edition, 1989.
Reference Source

17. Boyd R: **Nonlinear Optics**. Academic Press, 2nd edition, 2003.
Publisher Full Text

18. Montecchi M, Nichelatti E, Montereali RM, *et al.*: **Increase of refractive index induced by absorbing centres.** *Opt Quantum Electron.* 2004; **36**(1–3): 43–56.
Publisher Full Text

19. Yu PY, Cardona M: **Fundamentals of Semiconductors**. Springer, Berlin, 2001.
Reference Source

20. Schaefer ST, Gao S, Webster PT, *et al.*: **Absorption edge characteristics of GaAs, GaSb, InAs, and InSb.** *J Appl Phys.* 2020; **127**(16): 165705.
Publisher Full Text

21. Tauc J, Grigorovici R, Vancu A: **Optical properties and electronic structure of amorphous germanium.** *Phys Stat Sol.* 1966; **15**(2): 627–637.
Publisher Full Text

22. Cody GD, Brooks BG, Abeles B: **Optical absorption above the optical gap of amorphous silicon hydride.** *Solar Energy Mater.* 1982; **8**(1–3): 231–240.
Publisher Full Text

23. NREL: **Concentrating solar power projects**. 2019.
Reference Source

24. Montecchi M, Piegari A, Polato P, *et al.*: **Spectrophotometric characterization of homogeneous and inhomogeneous thin films for architectural glazing applications.** *Glass Technology.* 1994; **35**: 224–229.
Reference Source

25. Caccavale F, Coppola R, Menelle A, *et al.*: **"characterisation of sno$_2$ films on architectural glass by neutron reflectometry, sims, cems and spectrophotometry.** *J Non-Cryst Solids.* 1997; **218**: 291–295.
Publisher Full Text

26. Battaglin C, Caccavale F, Menelle A, *et al.*: **Characterisation of antire-flective TiO$_2$//SiO$_2$ coatings by complementary techniques.** *Thin Solid Films.* 1999; **351**(1–2): 176–179.
Publisher Full Text

27. Battaglin G, Menelle A, Montecchi M, *et al.*: **Neutron reflectometry for the investigation of multilayer coatings for building applications.** *Glass Technology.* 2002; **43**(5): 203–208.
Reference Source

28. Fernández-García A, Sutter F, Montecchi M, *et al.*: **Parameters and Method to Evaluate the Reflectance Properties of Reflector Materials for Concentrating So-lar Power Technology, V 3.1**. 2018.
Reference Source

29. Montecchi M: **Upgrading of enea solar mirror qualification set-up.** *Energy Procedia.* 2014; **49**: 2154–2161.
Publisher Full Text

30. Montecchi M, Sutter F, Fernández-García A, *et al.*: **Enhanced equivalent model algorithm for solar mirrors.** In: *AIP Conf Proc.* 2020; **2303**: 100005.
Publisher Full Text

31. Palik ED: **Handbook of Optical Constants of Solids**. Academic Press, 1985.

32. Chopra KL, Major S, Pandya DK: **Transparent conductors-a status review.** *Thin Solid Films.* 1983; **102**(1): 1–46.
Publisher Full Text

33. Cruz A, Erfurt D, Köhler R, *et al.*: **Industrial TCOs for SHJ solar cells: Approaches for optimizing performance and cost.** *Photovoltaics International.* 2020; **44**: 86–96.
Reference Source

34. Calnan S, Tiwari AN: **High mobility transparent conducting oxides for thin film solar cells.** *Thin Solid Films.* 2010; **518**(7): 1839–1849.
Publisher Full Text

35. Wang Y, Wenisch R, Schlatmann R, *et al.*: **Inorganic materials as hole selective contacts and intermediate tunnel junction layer for monolithic Perovskite-CIGSe tandem solar cells.** *Adv Energy Mater.* 2018; **8**(30): 1801692.
Publisher Full Text

36. Kam KK, Parkinson BA: **Detailed photocurrent spectroscopy of the semiconducting group VIB transition metal dichalcogenides.** *J Phys Chem.* 1982; **86**(4): 463–467.
Publisher Full Text

37. Wilson JA, Yoffe AD: **The transition metal dichalcogenides discussion and interpretation of the observed optical, electrical and structural properties.** *Adv Phys.* 1969; **18**(73): 193–335.
Publisher Full Text

38. Shimada T, Ohuchi FS, Parkinson BA: **Work function and photothreshold of layered metal dichalcogenides.** *Jap J Appl Phys.* 1994; **33**(5R): 2696–2698.
Publisher Full Text

39. Valentini M, Malerba C, Serenelli L, *et al.*: **Fabrication of monolithic CZTS/Si tandem cells by development of the intermediate connection.** *Solar Energy.* 2019; **190**: 414–419.
Publisher Full Text

Open Peer Review

Current Peer Review Status: ✔ ✔

Version 1

Reviewer Report 04 November 2021

https://doi.org/10.21956/openreseurope.14925.r27755

© **2021 Korte L et al.** This is an open access peer review report distributed under the terms of the Creative Commons Attribution License, which permits unrestricted use, distribution, and reproduction in any medium, provided the original work is properly cited.

✔ **Lars Korte**
[1] Young Investigator Group Perovskite Tandem Solar Cells, Helmholtz-Zentrum Berlin für Materialien und Energie GmbH, Berlin, Germany
[2] Young Investigator Group Perovskite Tandem Solar Cells, Helmholtz-Zentrum Berlin für Materialien und Energie GmbH, Berlin, Germany
Alvaro Tejada
[1] Young Investigator Group Perovskite Tandem Solar Cells, Helmholtz-Zentrum Berlin für Materialien und Energie GmbH, Berlin, Germany
[2] Departamento de Ciencias, Seccion Fisica, Pontificia Universidad Catolica del Peru, Lima, Peru
[3] Young Investigator Group Perovskite Tandem Solar Cells, Helmholtz-Zentrum Berlin für Materialien und Energie GmbH, Berlin, Germany
[4] Departamento de Ciencias, Seccion Fisica, Pontificia Universidad Catolica del Peru, Lima, Peru

The article describes the capabilities of the open source software “kSEMAW”, which is intended for the calculation of optical constants from measurements such as T, R, PDS and ellipsometry. As stated by the authors, the software has been extensively developed over many years and allows for the modelling and analysis of both ideal and non-ideal multi-layer stacks through Fresnel equations and the transfer matrix method. The article is based on the online manual for the software and depicts two different fitting methodologies: a point-by-point approach called the solution tracking method, and a hybrid method named IbridOne. Both are described in detail and are shown in action through various examples. There is also mention of the Equivalent Model Algorithm for obtaining angle-averaged values for T and R.

The article is scientifically sound and appears quite rigorous in its consideration of the underlying theory. It also demonstrates knowledge of the various experimental concerns and minutia that arise when working with different types of materials, gained through experience.

The implementation of the solution tracking method is praiseworthy as it highlights the common issues of point-by-point fitting and provides explicit insight on the various (and often diverging) solution branches for n and k. My only question on this matter is whether the film thickness can be

fitted using this method, i.e. can the software run through the entire wavelength range, vary the thickness, and try again, in order to minimize the “total” error?

The situation for the IbridOne algorithm, on the other hand, is a bit confusing. The examples highlight its benefits over the previous method (e.g. reduced sensitivity to instrument artifacts), however it is unclear how this approach is superior (or a suitable alternative) to directly modelling both n and k with oscillator functions, as most commercial software does. The method is quite unconventional in that it uses the dispersion model for only n to extract k from a T measurement, and then uses the R measurement to iteratively validate this. Because it numerically obtains k in this way, some issues become apparent:

1. In comparison to the solution tracking method, k will have the same disadvantages of susceptibility to noise in the measured data and possible unphysical behaviors, without the advantage of being unconstrained by a dispersion model (as the point-to-point models are). This seems like a “worst of both worlds” scenario.

2. Because the fit for T is perfect by definition, it is impossible to assess the quality of the fit with this measurement. Because T is very sensitive to low absorption values (e.g. near the bandgap), as opposed to R, I would say this is a disadvantage, as it makes it less obvious if there are issues with the optical model for the layer stack.

3. Because it is explicitly based on T and R measurements, it is not clear if this methodology could include (or be applied to) additional measurements like ellipsometry or PDS.

In fact, if both n and k were modeled, one would not run into issues such as the negative k in use case #2. Also, it would be possible to fit both n and k in use case #3.
I’d ask the author to address the previous points, clarify the rationale behind the IbridOne method, and justify its choice over more conventional approaches.
Finally, a couple of technical questions that could be clarified easily in a revised version of the manuscript:

1. Can the software combine different measurement types in a single fit? For example, if one has R, T and ellipsometry, can it use all of the datasets at once to further constrain the final solution?

2. Regarding the previous point, what happens if the wavelength values of the different datasets overlap but don’t match? For example, one dataset comes from a scanning monochromator with the wavelength values evenly spaced, and another dataset comes from a CCD array with irregular spacing?

Is the rationale for developing the new software tool clearly explained?

Partly

Is the description of the software tool technically sound?

Yes

Are sufficient details of the code, methods and analysis (if applicable) provided to allow replication of the software development and its use by others?

Yes

Is sufficient information provided to allow interpretation of the expected output datasets

and any results generated using the tool?
Yes

Competing Interests: No competing interests were disclosed.

Reviewer Expertise: solid state physics; semiconductor physics; physics and technology of thin film deposition and characterization; electronic and optical properties of semiconductors and TCOs; solar cells

We confirm that we have read this submission and believe that we have an appropriate level of expertise to confirm that it is of an acceptable scientific standard.

Author Response 16 Nov 2021

Marco Montecchi

Once again we would like to thank the two referees of this second round for their careful review. Our reply to each raised point is following. (Reviewer comments in italics)

My only question on this matter (the solution tracking method) is whether the film thickness can be fitted using this method, i.e. can the software run through the entire wavelength range, vary the thickness, and try again, in order to minimize the "total" error?
Author Reply: As discussed in User Case #2, the solution tracking method allows the user to optimize the film thickness by optimizing the solution-connection of the odd crossings. Please note that it is up to the user to manually adjust the thickness-value for improving the connections, by trial and error, following the indication reported in the papers [12,13] ; i.e. here the optimization is not automated. The accuracy of such thickness evaluation can be inferred by the thickness range for which the crossing is well connected.

1. (For the IbridOne method) In comparison to the solution tracking method, k will have the same disadvantages of susceptibility to noise in the measured data and possible unphysical behaviors, without the advantage of being unconstrained by a dispersion model (as the point-to-point models are). This seems like a "worst of both worlds" scenario.
Author Reply: The IbridOne method was introduced to obtain $k(\lambda)$ directly from the experimental data without a detailed model of all the physical mechanisms (excitons, defects, band tails etc) which can be involved in its behavior and which can produce a very articulated spectrum. In general instead $n(\lambda)$ shows a more regular behavior and therefore its modeling is less critical. In our opinion therefore IbridOne is not a "worst of both cases" but a different way to analyze the data: it is automated (while the tracking method is not) and it requires less assumptions than a method where both $n(\lambda)$ and $k(\lambda)$ are modeled and simultaneously fitted. In any case, we are working to add in kSEMAW the possibility to perform this latter (more conventional) fit-option.

2. (For the IbridOne method) Because the fit for T is perfect by definition, it is impossible to assess the quality of the fit with this measurement. Because T is very sensitive to low absorption values (e.g. near the bandgap), as opposed to R, I would say this is a disadvantage, as it makes it less obvious if there are issues with the optical model for the layer stack.

Author Reply: The referee objection is correct if the goal of the analysis is to obtain a detailed physical model of the optical properties of the investigated material. On the other hand the main goal of the IbridOne method is to obtain numerical values of $n(\lambda)$ and $k(\lambda)$ useful for the applications of the material. As for the assessment of the fit quality we point out that the IbridOne method returns also the errors on $n(\lambda)$ and $k(\lambda)$ calculated on the basis of the experimental errors on T and R.

3. (For the IbridOne method) Because it is explicitly based on T and R measurements, it is not clear if this methodology could include (or be applied to) additional measurements like ellipsometry or PDS.
Author Reply: Currently the IbridOne method can use only the spectrophotometric measurements for T and R (also measured at oblique incidence, polarized or not and from both sample sides). A future implementation of the method will be the possibility to replace R with the ellipsometric angle Psi which in the space (n,k) has a similar behavior and to replace T with the PDS data.

Reply to the technical questions

1. Can the software combine different measurement types in a single fit? For example, if one has R, T and ellipsometry, can it use all of the datasets at once to further constrain the final solution?
Author Reply: Currently different measurement types can be used together in the tracking method to obtain the (n,k) solution set. As stated above this is not possible for the IbridOne method in the current version but it will be implemented in the next future.

2. Regarding the previous point, what happens if the wavelength values of the different datasets overlap but don't match? For example, one dataset comes from a scanning monochromator with the wavelength values evenly spaced, and another dataset comes from a CCD array with irregular spacing?
Author Reply: Different wavelength spacing in the different datasets is not a problem since the first operation performed by kSEMAW is the resampling of the input data on a common wavelength set.

Competing Interests: No competing interests were disclosed.

Reviewer Report 21 September 2021

https://doi.org/10.21956/openreseurope.14925.r27647

© 2021 Zanotto S. This is an open access peer review report distributed under the terms of the Creative Commons Attribution License, which permits unrestricted use, distribution, and reproduction in any medium, provided the original work is properly cited.

Simone Zanotto
[1] CNR - Istituto di Nanoscienze, Pisa, Italy

[2] CNR - Istituto di Nanoscienze, Pisa, Italy

The article "KSEMAW: an open source software for the analysis of spectrophotometric, ellipsometric and photothermal deflection spectroscopy measurements", by M. Montecchi, A. Mittiga, C. Malerba, and F. Menchini illustrates the features of a computer program originally developed for in-house use, and later extended to be exploitable by a larger public including academic and industrial researchers in the fields of optical coating.

The article recalls the contents of the software user manual, available in the GitHub repository, adding several cases of study, and information about the Equivalent Model Algorithm (EMA) [page 12], that however seems quite off-topic with respect to the main thread of the article.

Concerning the contents, the article looks complete and scientifically sound, describing the theoretical methods and the numerical implementation. Software installation procedures are better explained in the online manual. The manuscript also provides lengthy analytical expressions for the permittivities; I have checked the consistency between the formulas reported in the article and those reported in the source code only in few cases.

A few points of the article resulted however slightly unclear to me:

1. How can the software user analyze the data from a photothermal deflection experiment?

2. Is it possible to fit simultaneously the n&k data of multiple layers of the coating under analysis? More in general, is it possible to define as fitting parameters a given subset of all the parameters describing the multilayer (e.g., the thickness of a certain layer, and the Lorentz oscillator frequencies of another layer)?

3. What are the "M_i_cal(n,k)" and similar quantities in the formula for the merit function (MF) [page 5]?

Finally, could the authors highlight the rationale behind the proposed implementation, possibly commenting on the differences/similarities between the proposed code/method, and that published under the name of "RegressPro", available as open-source code at https://github.com/franko/regress-pro?

Is the rationale for developing the new software tool clearly explained?

Partly

Is the description of the software tool technically sound?

Yes

Are sufficient details of the code, methods and analysis (if applicable) provided to allow replication of the software development and its use by others?

Yes

Is sufficient information provided to allow interpretation of the expected output datasets and any results generated using the tool?

Yes

Competing Interests: No competing interests were disclosed.

Reviewer Expertise: Photonics, metamaterials

I confirm that I have read this submission and believe that I have an appropriate level of expertise to confirm that it is of an acceptable scientific standard.

Author Response 30 Sep 2021

Marco Montecchi

First of all we would like to thank the referee for his careful review of the paper. Our reply to the comments follows.

1. *How can the software user analyze the data from a photothermal deflection experiment?*

   The file containing the PDS data can be loaded in the same way as the spectrophotometric and ellipsometric data. After that, the user can simply simulate the PDS data providing an optical model defined by the layer thicknesses and the material refractive indexes. The refractive indexes can be provided as input data files as well as oscillators sets. All the parameters can then be manually optimized to reproduce the experimental data. On the other hand, if the user wants to obtain the refractive index using the solution-tracking or the IbridOne method, the PDS data must be accompanied by another data file as reflectance or Ψ from ellipsometric measurement.

2. *Is it possible to fit simultaneously the n&k data of multiple layers of the coating under analysis? More in general, is it possible to define as fitting parameters a given subset of all the parameters describing the multilayer (e.g., the thickness of a certain layer, and the Lorentz oscillator frequencies of another layer)?*

   In the current version the user can fit the unknown complex refractive index of just one material described by a given set of oscillators. On the other hand, the unknown material can be associated to more than one layer and any other parameter of each layer (thickness, roughness, *n*-gradient, etc) can be defined by the user as a fitting parameters.

3. *Are the "M_i_cal(n,k)" and similar quantities in the formula for the merit function (MF) [page 5]?*

   The merit function MF defined in page 5 refers to a single wavelength value. The index i runs on the considered experimental measurements M_i_exp (typically R and T). M_i_cal(nk) is the value of the M_i measurement calculated using the (n,k) values.

Rationale:

kSEMAW is a new open source software for thin film characterization finally published after about 30 years of development and private use. The software has already been used in various fields of physics, such as thin film optical filters, architectural glazing, detectors for

high energy physics, solar energy, and, last but not least, photovoltaic devices. Since the beginning, the software has been conceived to be used by people involved in both growth process and optical characterization of thin film, for which the determination of thickness and complex refractive index of a film is crucial. kSEMAW can load all the most relevant measurements for thin film characterization, such as spectrophotometry (transmittance and reflectance, at near-normal as well as oblique incidence), ellipsometry and Photo-Thermal-Deflection spectroscopy. kSEMAW manages optical models consisting of up to 9 layers; eventually roughness, gradient and/or curvature of index profile across the film thickness can be individually set for each one of the 9 layers. Beside the unknown materials, the refractive index of all the other materials can be provided by numerical data files or by setting a suitable ensemble of oscillators. The unknown refractive index can be evaluated in two different ways: 1) numerically, lambda by lambda (solution-tracking method); 2) best fit of reflectance once the extinction coefficient is evaluated by the transmittance (IbridOne method). In the latter method the refractive index can be modeled by a suitable number of oscillators selected among nine different types. The underlined subjects in the rational are not present in the other open-source software Regress Pro. An important difference between the two softwares concerns the oscillator types available for the fitting procedure. In Regress Pro they are only three: • Cauchy • Lorentz • Tauc-Lorentz We note that the Cauchy oscillator is just an heuristic function and the Tauc-Lorentz oscillator is based on a epsilon_2 proportional to (E-Eg)^2/E^2 which is suitable for amorphous or indirect-gap semiconductors but not for direct gap materials. KSEMAW instead has a richer assortment of oscillators suitable for both direct and indirect gap materials: • Flat • Lorentz • Quant-homo • Quant-inhomo • Drude • Direct Gap Cody • Direct Gap Tauc • Indirect Gap Cody • Indirect Gap Tauc Finally we want to point out that the broadening effect in the Tauc-Lorentz oscillator used by Regress Pro is obtained by a simple multiplication by a Lorentz oscillator centered on the maximum of the joint density of states while in kSEMAW the same effect is obtained by convolution with a single oscillator epsilon_2 which is more physically sensible.

Competing Interests: No competing interests were disclosed.